applied sciences

MDPI

Article

Targeting TGF-ß in the Central Nervous System: Assessment of Cynomolgus Monkey—Toxicity and Pharmacokinetics for an LNA-Antisense Oligonucleotide

Sebastian Peters [1], Eva Wirkert [1], Sabrina Kuespert [1], Rosmarie Heydn [1], Sven Korte [2], Lars Mecklenburg [2], Ludwig Aigner [3], Siw Johannesen [1,†], Tim-Henrik Bruun [1,‡] and Ulrich Bogdahn [1,*,‡]

[1] Department of Neurology, University Hospital Regensburg, 93053 Regensburg, Germany; sebastian.peters@velvio.com (S.P.); eva.wirkert@velvio.com (E.W.); sabrina.kuespert@velvio.com (S.K.); Rosmarie.Heydn@velvio.com (R.H.); siw.johannesen@bgu-murnau.de (S.J.); tim-henrik.bruun@velvio.com (T.-H.B.)
[2] Labcorp Early Development Services GmbH, 48163 Muenster, Germany; sven.korte@labcorp.com (S.K.); Lars.mecklenburg@labcorp.com (L.M.)
[3] Institute of Molecular Regenerative Medicine, Spinal Cord Injury and Tissue Regeneration Center Salzburg (SCI-TReCS), Paracelsus Medical University Salzburg, 5020 Salzburg, Austria; ludwig.aigner@pmu.ac.at
* Correspondence: ulrich.bogdahn@velvio.com
† Current address: BG Trauma Center, Professor Küntscher Str. 8, 82418 Murnau (Staffelsee), Germany.
‡ Current address: Velvio GmbH, Am Biopark 11, 93053 Regensburg, Germany.

Citation: Peters, S.; Wirkert, E.; Kuespert, S.; Heydn, R.; Korte, S.; Mecklenburg, L.; Aigner, L.; Johannesen, S.; Bruun, T.-H.; Bogdahn, U. Targeting TGF-ß in the Central Nervous System: Assessment of Cynomolgus Monkey—Toxicity and Pharmacokinetics for an LNA-Antisense Oligonucleotide. *Appl. Sci.* **2022**, *12*, 973. https://doi.org/10.3390/app12030973

Academic Editors: Jessica Ceramella and Domenico Iacopetta

Received: 17 November 2021
Accepted: 12 January 2022
Published: 18 January 2022

Abstract: Increasingly antisense oligonucleotides (ASOs) are developed for potential treatment of CNS disorders, and due to the inability to cross the blood brain barrier, they require direct administration into the cerebrospinal fluid (CSF). In this regard, intrathecal (i.th.) administration in cynomolgus monkeys (*Macaca fascicularis*) is a well-established approach for preclinical safety studies. Here, we present an innovative preclinical approach that is intended to support rapid entry into clinical development with ASOs targeting the CNS. The preclinical approach comprises one non-GLP study in 26 non-human primates, followed by a pivotal GLP repeated dose toxicity study in the same species. No pivotal rodent studies were conducted, and regulatory guidance to initiate this study was met by in vitro work. The non-GLP study consists of three separate phases: Phase A determines toxicity after i.th. administrations with five escalating dose levels in a single male and female animal, respectively. Dosing is conducted on days 1, 8, 15, 22, and 29 and the experiment is terminated 36 days after start of the study. The second phase (Phase B) investigates pharmacokinetics over a 2- or 4-week period at two dose levels following single administrations in eight (8) animals (4 females, 4 males). Finally, a third phase (Phase C) investigates toxicity and pharmacokinetics after repeated (9×) dosing over a 13-week period at two dose levels in sixteen (8 females, 8 males) animals. In each phase, clinical observations and physical/neurological parameters are investigated directly pre-dose, 4 h and 24 h post-dose, respectively. In all phases, CSF and blood samples are taken pre-dose and after each dosing, for determination of test article concentration, biomarkers of tolerability and biomarkers of pharmacology. In all phases, tissue samples from the liver, kidney, spinal cord, and brain are collected for determination of NVP-13 tissue concentrations. The above concept has successfully supported first-in-human clinical trials. The entire non-GLP program is completed within less than six months and requires fewer animals in comparison to the conduct of three independent studies.

Keywords: antisense oligonucleotide therapy; LNA; TGFß-signaling; neurodegeneration; ALS

1. Introduction

Oligonucleotide therapies are currently experiencing a resurgence, driven by advances in backbone chemistry and discoveries of novel therapeutic pathways that can be uniquely

and efficiently modulated by oligonucleotide drugs. A quarter of a century has passed since oligonucleotides were first administered to brains of living mammals to modulate gene expression. Despite challenges in non-systemic local delivery, multiple oligonucleotide-based compounds are currently delivered for treatment of central nervous disorders by direct intrathecal (i.th) administration—to circumvent a more or less intact blood brain barrier [1–5].

The most prominent candidate is Spinraza™ (Nusinersen), a new treatment of spinal muscular atrophy (SMA), which was supported by safety assessment of chronic i.th bolus delivery in cynomolgus monkeys (*Macaca fascicularis)* [6–9].

The disequilibrium of neuroregeneration and neurodegeneration with a shift towards the latter, and a premature neuronal loss in specific brain areas is one major characteristic of neurodegenerative disorders, independent of the individual patient's genetic disease background. Preceding disease manifestation, neuronal loss is compensated at least in earlier disease stages by suitable cell replacement (e.g., by increased neurogenesis) [10–13]. In neurodegenerative disorders or even in aged patients, a multitude of partly known causes lead to enhanced inflammation and, among other cytokines, to increased TGF-ß concentrations in parenchyma and CSF [14–17]. The excess of TGF-ß heavily activates TGF-ß signaling pathways in cells positive for TGFBR2. Crucially, among cells positive for this receptor are neuronal progenitor stem cells, which respond on this exaggerated TGF-ß signaling by decreasing cell division [18]. However, these stem cells are essential for a physiological replacement mechanism (e.g., pathological motor neuron decay, as in ALS). TGFBR2 as essential ligand binding receptor is the key element to activate the TGF-ß signaling cascades. Targeting the mRNA of TGFBR2 also results in protecting neuronal stem cells from cell cycle arrest in their physiological proliferation and conclusively in brain repair mechanism. Other relevant mechanisms addressed by targeting the TGFBR2 are immune regulation, extracellular matrix and fibrosis, which may contribute to the neurodegenerative process [19,20], and finally, autophagy.

In order to dampen an exaggerated TGFBR2-mediated signaling, we developed a novel LNA-Gapmer ASO. Previous in vitro and in vivo studies demonstrate a safe, low toxic, and highly efficient profile of this drug candidate [21,22].

As described above, many antisense oligonucleotide (ASOs) drugs are developed for neuronal disorders. Due to the inability to cross the blood brain barrier, ASOs require direct administration into the cerebrospinal fluid (CSF): i.th. bolus delivery in cynomolgus monkeys is a preferred method in preclinical safety assessment of central nervous system (CNS) drugs [23,24]. Occasionally, port-catheterization is preferred for overcoming some more specific pharmacokinetic limitations [25–27].

ASOs are chemically synthesized and generally require preclinical safety testing in a rodent and a non-rodent species. Yet, they may show limited or even absent pharmacological activity in rodents and thus may be tested in non-rodents only. The cynomolgus monkey is the preferred non-rodent species for ASO safety testing, because many potential drugs against neurodegenerative diseases, particularly antisense oligonucleotides (ASOs), are administered via lumbar i.th. injection, as they do not efficiently cross the blood-brain barrier. This route is well established in cynomolgus monkeys that are commonly used for preclinical safety assessment when other nonrodent species such as dog or minipig cannot be used. Typically, a preclinical safety program for a novel ASO drug candidate comprises a maximum-tolerated-dose (MTD) study, a study addressing the pharmacokinetic profile of the drug, a non-GLP repeated dose study to determine a suitable dose range, and finally, a pivotal GLP-compliant repeated dose toxicity study. Here, we present a novel approach towards preclinical safety testing of ASOs targeting the CNS in the scope of a first-in-human clinical trial.

This preclinical approach consists of only two studies. The first study is conducted under non-GLP conditions and comprises three phases conducted in only 26 animals. This study is then followed by a GLP-compliant repeated dose toxicity study as described elsewhere [28]. No pivotal toxicity testing was conducted in rodents, but non-specific

toxicity was tested in mice, and drug efficacy was evaluated by in vitro work [21]. The presented study design was successfully implemented in an antisense design project to support rapid entry into clinical development. The objectives of the study were (a) to determine the maximum tolerated dose of the test item, NVP-13, following intrathecal administrations in Phase A, (b) to determine the pharmacokinetics of the test item after i.th. application in Phase B, and (c) to determine the dose-range for a 13-week GLP repeated intrathecal dose toxicity study.

2. Materials and Methods

2.1. Animals

Male (n = 13) and female (n = 13) (Phase A: Male (n = 1) and female (n = 1); Phase B: Male (n = 4) and female (n = 4); Phase C: Male (n = 8) and female (n = 8)). Cynomolgus monkeys (*Macaca fascicularis*, supplied from a self-sustaining colony in Asia (Nafovanny Tam Phuoc Ward, Bien Hoa City, Dong Nai Province, Vietnam)), with the age of 2 to 6 years, weighing 2.2 to 5 kg were housed in groups of 3 animals. The animals were randomized to treatment groups to ensure equal bodyweight per group and sex. All animals were kept in an AAALAC accredited facility under standard laboratory conditions in a climate-controlled room with a minimum of 8 air changes/hour (12-h light/dark cycle, 19 to 25 °C, 40 to 70% humidity). All animals received a certified lab diet for primates (LabDiet 5048) twice daily, supplemented by fresh fruits and vegetables and had access to tap water (H_2O) ad libitum. Immediately after each handling/manipulation, the animals received a tasty reward. All experimental procedures are in compliance with the German Animal Welfare Act and are approved by the local IACUC. The study was approved by the local authority (Landesamt für Natur, Umwelt und Verbraucherschutz, NRW) and registered under following file number: 84-02.04.2017.A093. This study was performed in compliance with the following guidelines or recommendations concerning preclinical development of human pharmaceuticals:

- European Directive 2001/83/EC and all subsequent amendments;
- German Drug Law;
- International Conference on Harmonization (ICH) Guideline: Guidance on Non-clinical Safety Studies for the Conduct of Human Clinical Trials and Marketing Authorization for Pharmaceuticals, M3(R2), issued in EMA as CPMP/ICH/286/95.

2.2. Antisense Oligonucleotide (NVP-13)

NVP-13, a 16-mer Gapmer LNA-Antisense Oligonucleotide was designed as the drug candidate to specifically hybridize with the mRNA for TGFBR2 [21]. The ASO exerts no cross-reactivity in rodents, dogs or minipigs, due to this high specificity. Therefore, non-human primates such as the cynomolgus monkeys had to be used for preclinical testing. Dose levels in this study were based on in vitro data (human neuronal progenitor cells) [21] and on recently published data for the treatment of spinal muscular atrophy (SMA) [6–9]. The LNA ASO targeting TGFBR2 of this study has chemical class similarity with the 2-MOE ASO Nusinersen of the published SMA data. The route of administration was chosen because it is the intended human therapeutic route.

2.3. Test System Justification

The ASO being investigated in this particular study is highly specific for the human target TGFBR2 message and consequently is only effective in humans and monkeys (species specific). The ASO exerts no cross-reactivity in other species, including rodents, due to this high specificity. Therefore, cynomolgus monkeys must be used.

2.4. Test Item

NVP-13 (Biospring Frankfurt, Batch 249403, under license of Exiqon) was delivered as a lyophilized powder and was formulated in accordance to mixing procedures provided by the Sponsor, using 0.9% Sodium Chloride for Injection. Artificial CSF (aCSF, from R

AND D SYSTEMS INC., Minneapolis, MN, USA) was used to flush the test or control item (vehicle) after dosing.

2.5. Dose Administration and Rationale

The rationale for the selection of dose levels in Phase A was based on our own in vitro data (human neuronal progenitor cells [21]) and on recently published data for the treatment of spinal muscular atrophy [6,9,29,30]. The LNA ASO targeting TGFBR2 of this study has strong chemical similarity with the 2-MOE ASO Nusinersen of the published SMA data. Therefore, the dose-escalation scheme in Phase A was in close relationship to those published data. Doses for Phases B and C were adapted with respect to results of Phase A. The high dose for Phase C aimed to produce target organ toxicity or non-specific toxicity. The intermediate dose for Phase C was the geometric mean of the low and high doses, and the low dose should have produced a pharmacodynamic effect, the desired therapeutic effect, or CSF levels similar to those expected in humans.

2.6. Dosing Procedure

For intrathecal dosing, animals were fasted and anesthetized with ketamine and medetomidine. After disinfecting the skin, a micro incision of the skin was conducted using a 20G needle. A pencil-point needle for pediatric use (Pencan Paed® needle, 25 G, B. Braun Melsungen AG, 34212 Melsungen, Germany) was then inserted at L4/L5 until CSF flow was observed (L3/4, L2/L3 were used if no CSF flow was observed). A volume of 0.5 mL CSF was removed for analytical purposes and to adjust for the volume addition by the test article. Thereafter, 0.75 mL of test article or aCSF (artificial cerebrospinal fluid; aCSF, from R AND D SYSTEMS INC) were injected over approximately 1 min, followed by a 0.25 mL flush with aCSF to empty the needle (Figure 1B). Needle and syringe were left in the dosing site for at least 30 s after the aCSF flush. Bepanthen® aseptic wound ointment (contains chlorhexidine and dexpanthenol) was applied immediately after each dosing. Thereafter, the animal was placed in a lying position for 15 min before the antidote was applied.

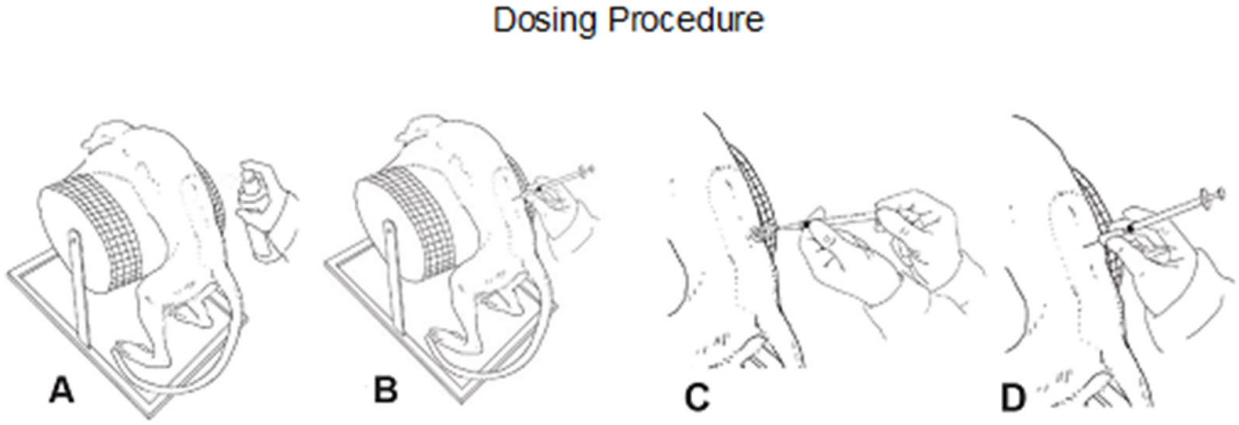

Figure 1. Schematic illustration of the dosing procedure. Following disinfection (**A**), intrathecal (i.th.) administration was performed via lumbar puncture between L3–L5 (**B**) by slow manual bolus infusion over 1 min to anesthetized animals. The needle (with syringe) was left in the dosing site for at least 30 s after aCSF flush. It was documented that CSF flow was present before dosing (**C**), that the position of the needle opening was facing towards the head of the animal prior to dose administration, and that the needle (with syringe) was left in dosing site for at least 30 s after aCSF flush (**D**).

2.7. Study Design

In **Phase A (tolerability/dose escalation)**, one male (Animal P0001M) and one female (Animal P0101F) of Group 1 were dosed once weekly on Days 1, 8, 15, 22, and 29, with

five escalating doses (0.4, 0.8, 4, and 20 mg/animal). After 5 weeks, these animals were sacrificed on Day 36 (Figure 2, Phase A).

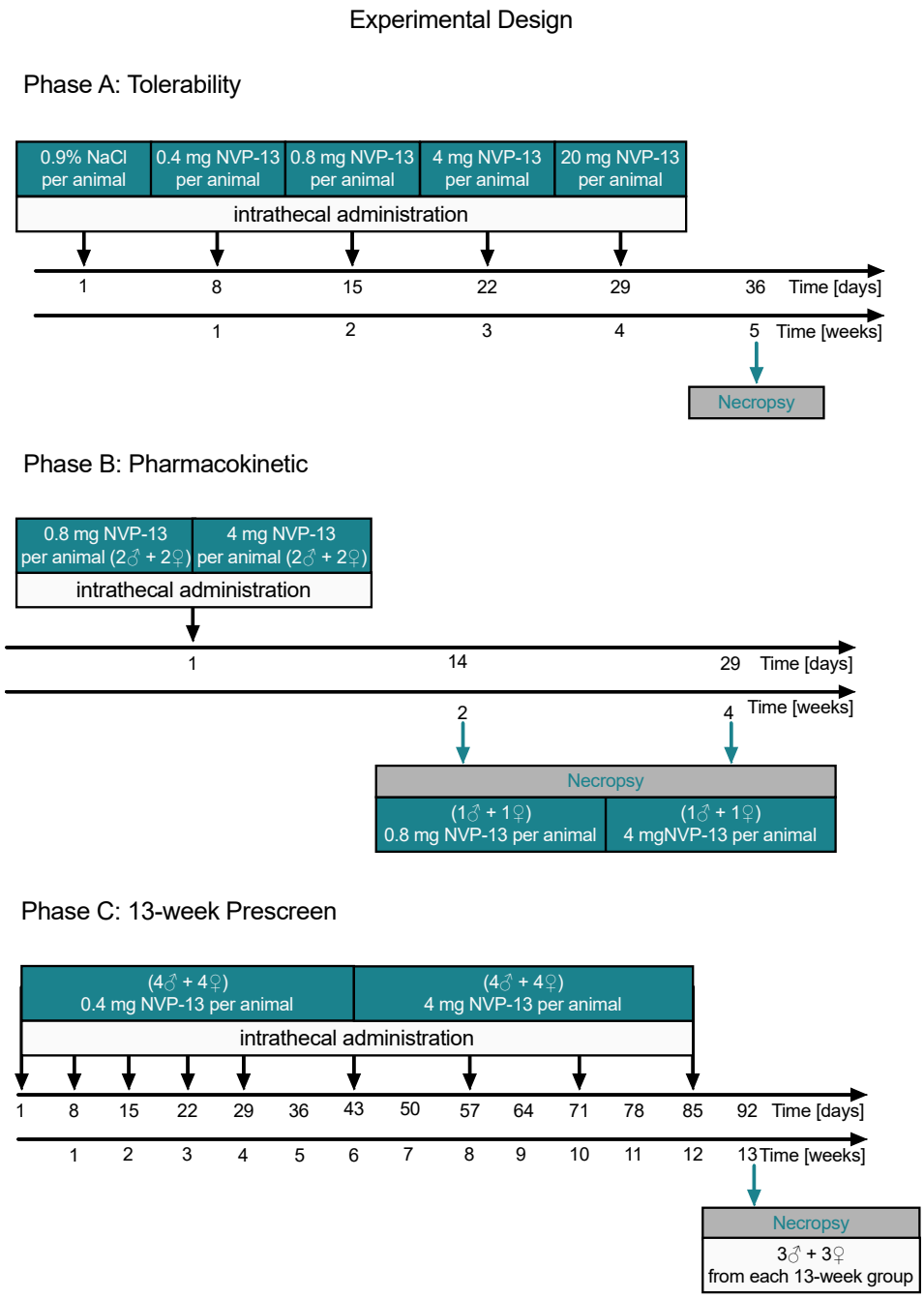

Figure 2. Schematic illustration of the experimental designs (Phases A–C). NVP-13 tolerability was evaluated by using a dose-escalation paradigm with increasing dose levels every single week (0.4 mg/animal to 20 mg/animal). One male and female Cynomolgus monkey received an intrathecal NVP-13 injection and physical/neurological parameters were investigated directly and following 4 h after administration (**Phase A**). In a second experiment, NVP-13 pharmacokinetics (**Phase B**) was evaluated via bioanalytical determination of NVP-13 tissue concentrations following 2 or 4 weeks of a single intrathecal drug administration for the two different NVP-13 doses (low: 0.8 mg/animal; high: 4 mg/animal). CSF was taken to evaluate NVP-13 half-life. Further, CNS tissue samples (spinal cord, brain) were collected to evaluated tissue distribution. Finally, in a third paradigm (**Phase C**), NVP-13 was injected repeatedly over a 13-week (9×) approach at two different doses (0.4 and 4 mg) to simulate a long-time administration period and to investigate possible NVP-13 saturation levels.

In **Phase B (pharmacokinetics)**, animals were dosed once on Day 1 with 0.8 mg/animal (Groups 2 and 3) or 4 mg/animal (Groups 4 and 5). One animal/sex/group was used in Groups 2 through 5. After 2 weeks, animals of Groups 2 and 4 were sacrificed on Day 14. After 4 weeks, animals of Groups 3 and 5 were sacrificed on Day 29 (Figure 2, Phase B).

In **Phase C (dose-range finding for toxicity)**, animals were dosed weekly for the first 4 weeks of that phase and every other week thereafter (nine doses total)—(on Days 1, 8, 15, 22, 29, 43, 57, 71, and 85 of Phase C). Phase C was conducted with four animals/sex/group. Group 6 animals were administered 0.4 mg/animal, and Group 7 animals were administered 4 mg/animal. After 13 weeks, both groups were sacrificed on Day 91 (Figure 2, Phase C).

2.8. Plasma Collection

Blood samples (total: 4.3 mL per animal; 1.3 mL for toxicokinetic examination and 3.0 mL for clinical chemistry) were collected from the *vena cephalica antebrachii* or *vena saphena* into K_2EDTA tubes from all animals. Blood samples were gently mixed by hand and were stored on crushed ice prior to centrifugation. Plasma was obtained by centrifugation at 4 °C and approximately 2300× *g* for 10 min. The plasma was aliquoted into four labeled micro tubes (three aliquots with at least 0.1 mL each and one aliquot with the remaining fluid) and stored frozen at −70 °C or below.

2.9. Cerebrospinal Fluid Collection

The CSF samples (approximately 0.3 mL, at the 24-h time point only 0.25 mL) were collected by lumbar puncture from fasted and anesthetized animals into micro-tubes (Sarstedt G & Co. KG, Sarstedtstraße 1, 51588 Nümbrecht, Germany) at multiple time points using the same spinal needle as for dosing. The CSF samples were sunk into liquid nitrogen immediately after sampling and stored at −70 °C or below.

2.10. Tissue Collection

(A) Brain: The brain was sectioned in a brain matrix at 4-mm coronal slice thickness. Each coronal slice was further divided sagittally into right and left hemispheres. The left hemisphere was preserved in 10% neutral buffered formalin for processing and microscopic evaluation. The right hemisphere was frozen at −70 °C for bioanalytical, mRNA, and biomarker analysis.

(B) Spinal Cord: The spinal cord was divided into cervical, thoracic, and lumbar sections. Each section was further divided into two portions. A 3-cm portion from the rostral end of each section was frozen at −70 °C for bioanalytical, mRNA, and biomarker analysis, and the remaining portion was fixed in 10% neutral-buffered formalin for microscopic evaluation. In addition, a section for histology was taken proximal to the injection site (e.g., between L3 and L4).

(C) Liver and Kidney: The liver (left lobe) and the kidney (*cortex* and *medulla*) were harvested. Samples of liver and kidney were split into two of 0.25 g each; samples were frozen at −70 °C or below for bioanalytical analysis.

2.11. Clinical Observations

Throughout the entire study, all animals were observed twice a day for any signs of ill health or overt toxicity (clinical observations). In addition, animals were clinically examined in detail once a week. Feces were evaluated daily.

2.12. In-Life Parameters

Standard in-life parameters included body weight, food consumption, physical and neurologic examinations, neurobehavioral observations, and ophthalmic observations were performed on regular timepoints throughout the entire experimental time of each phase.

2.13. Clinical Pathology

Blood samples (3.0 mL) were withdrawn from all animals once during the pre-dose phase, during Week 13 of the dosing phase, and from all surviving animals during the last week of the recovery phase. Samples were collected from the *vena cephalica antebrachii* or *vena saphena* and hematology tests (Table 1), coagulation tests, and clinical chemistry tests (Table 2) were performed.

Table 1. Summary of hematological parameters investigated throughout every phase withing the experiment.

Code	Parameter	Method of Determination
HGB.	Hemoglobin	SLS (Sodiumlaurylsulfate)—Hemoglobin Method
RBC.	Red Blood Cells	Electric Resistance Detection
HCT.	Hematocrit	Calculated via the RBC. Pulse Height Detection
MCV.	Mean Corpuscular Volume	Calculated from RBC. and HCT.
MCH.	Mean Corpuscular Hemoglobin	Calculated from RBC. and HGB.
MCHC.	Mean Corpuscular Hemoglobin Concentration	Calculated from HGB. and HCT.
RETI.	Reticulocytes ‰	Flow Cytometry
TRET.	Absolute Reticulocytes	Flow Cytometry
WBC.	White Blood Cells	Flow Cytometry
ANEU.	Neutrophils	Calculation
ALYM.	Lymphocytes	Calculation
AMON.	Monocytes	Calculation
AEOS.	Eosinophils	Calculation
ABAS.	Basophils	Calculation
NEUT.	Neutrophils %	Flow Cytometry
LYM.	Lymphocytes %	Flow Cytometry
MONO.	Monocytes %	Flow Cytometry
EOS.	Eosinophils %	Flow Cytometry
BASO.	Basophils %	Flow Cytometry
PLT.	Platelets	1. Electric Resistance Detection (Impedance)/ 2. Optical Count (PLT-O)

2.14. End of In-Life Phase

All animals were subjected to necropsy. All animals were fasted overnight prior to scheduled necropsies. Where possible, necropsies were carried out in replicate in order to ensure equal numbers of animals from each group and/or sex were sacrificed on each day. Animals were administered an intramuscular injection of ketamine hydrochloride, which was followed by an intravenous overdose of sodium pentobarbitone prior to exsanguination.

2.15. Necropsy, Organ Weights, and Macroscopic Observations

A full macroscopic examination was performed under the general supervision of a Pathologist, and all findings were recorded.

2.16. Histology

Brain, spinal cord, liver, kidney, and lymph node tissue from each animal were trimmed and embedded in paraffin wax, sectioned at a nominal 5 µm, stained with hematoxylin and eosin and analyzed for microscopic alterations. Sectioning of the brain was performed such that, at a minimum, the following structures were captured: neocortex (including frontal, parietal, temporal and occipital cortex), paleocortex (olfactory bulbs and/or piriform lobe), basal ganglia (including caudate and putamen), limbic system (including hippocampus and cingulate gyri), thalamus/hypothalamus, midbrain regions including substantia nigra, subventricular zone, cerebellum, pons, and medulla oblongata.

Table 2. Summary of clinical chemistry parameters investigated throughout every phase throughout the experiment.

Code	Parameter	Method of Determination
AST.	Aspartate Aminotransferase	IFCC Reference Method with Pyridoxal Phosphate Activation
ALT.	Alanine Aminotransferase	IFCC Reference Method with Pyridoxal Phosphate Activation
ALP.	Alkaline Phosphatase	Colorimetric Method using p Nitrophenyl Phosphate as Substrate Standardized to IFCC
CHOL.	Total Cholesterol	Enzymatic Method using Cholesterol Oxidase/Esterase
TRIG.	Triglycerides	Enzymatic Method using Lipase and Glycerol Kinase as Primary Enzymes
TBIL.	Total Bilirubin	A colorimetric Method (Malloy-Evelyn) in which indirect Bilirubin is liberated by Detergent. Total Bilirubin is then coupled with a Diazonium Compound to give Corresponding Azobilirubin.
TP.	Total Protein	Biuret Method
ALB.	Albumin	Colorimetric Method using Bromocresol Green
GLOB.	Globulin	Calculation (Globuli*n* = Total protein − Albumin)
A:G.	Albumin/Globulin Ratio	Calculation (Albumin/Globulin)
NA.	Sodium	Ion Selective Electrode (Direct Potentiometric)
K.	Potassium	Ion Selective Electrode (Direct Potentiometric)
CL.	Chloride	Ion Selective Electrode (Direct Potentiometric)
CA.	Calcium	Colorimetric Method using Arsenazo III
PHOS.	Inorganic Phosphorus	UV Method using Ammonium Molybdate
CREA.	Creatinine	Colorimetric Method using Picric Acid (Standard Jaffe Method)
BU.	Blood Urea	UV Method using a coupled Urease Procedure
GLDH.	Glutamate Dehydrogenase	UV Method with optimized Substrate Concentration (Optimized DGKC Method)
GGT.	Gamma Glutamyltransferase	Standardized IFCC colorimetric Method
GLU.	Glucose	UV Method using a Coupled Hexokinase Procedure

2.17. Microscopic Observations

Tissues were examined microscopically by a pathologist.

2.18. NVP-13 Concentration Measurement

Plasma: The analytical work was done in accordance to standard operating procedures and for each chromatographic analysis batch, a detailed assay protocol was generated and retained as raw data. The method was validated at Axolabs prior to the start of this study phase. Results of the method validation are summarized in the Method Validation Report for the PNA-HPLC-Assay for cynomolgus monkey plasma: AN57.0-17.

The analytical method is based on an AEX-HPLC method with fluorescence detection that allows the sensitive and specific detection of NVP-13 from cynomolgus monkey plasma samples. The assay is based on the specific hybridization of a 16-mer complementary PNA-probe conjugated at the N-terminus with Atto425 dye. The duplex of PNA and parent compound yields a specific signal in the subsequent analysis by AEX-HPLC coupled to a fluorescence detector, as described in detail earlier [21]. Quantification is performed based on an external calibration curve generated from a standard dilution series in cynomolgus monkey plasma. Linear calibration curves (weighted 1/X) are calculated from 1 ng/mL to 5000 ng/mL.

CSF: The method of analysis used in this study is documented in Standard test Method: STM_NVP-13_CynoCSF. The analytical work was done in accordance with Axolabs' SOP

RA-001 and for each chromatographic analysis batch, a detailed assay protocol was generated and retained as raw data. The method was validated at Axolabs prior to the start of this study phase. Results of the method validation are summarized in the Method Validation Report for the PNA-HPLC-Assay for cynomolgus monkey plasma: AN58.0-17.

The analytical method is based on an AEX-HPLC method as described above (Plasma section) using cynomolgus CSF instead of plasma for calibration.

Tissue: The method of analysis used is documented in the Method Development Report: MDR NVP-13 & 19_PNA-HPLC-Assay. The analytical work was done in accordance to SOP RA-001 and for each chromatographic analysis batch, a detailed assay protocol was generated and retained as raw data. The method was qualified previously at Axolabs under Method Development Project No. AN479.0-15 prior to the start of this study.

Details on all mentioned protocols and reports may be provided by the corresponding author upon reasonable request.

2.19. Statistics

Due to low animal number in Phases A and B, statistical analysis was only performed in Phase C. For graph design and statistical comparison, GraphPad Prism 8 was employed. All parameters were tested for Gaussian distribution using the D'Augostino–Pearson omnibus normality test or the Shapiro–Wilk normality test (samples sizes too small for the D'Augostino–Pearson omnibus normality test). Afterwards, all parameters were analyzed using a one-way ANOVA followed by Tukey post hoc test or a Kruskal–Wallis test followed by Dunn's post hoc test, depending on Gaussian distribution. Data are presented as median with min to max or mean ± SEM depending on statistical analysis. Significance was taken at $p \leq 0.05$.

3. Results

Phase A: Dose levels were escalated from 0.4 mg/dose to 20 mg/dose. The only adverse test item-related finding was observed at a dose level of 20 mg/animal:

The Phase A female (Animal P0101F) was prematurely sacrificed on Day 29 due to apparent neurological findings at 20-mg dose (paralysis of arms and legs, missing tendon reflexes). In autopsy, no microscopic correlate to this finding could be identified. A test item-related finding of neuronal vacuolation was noted in the cerebral cortex and hippocampus of this animal's brain; this finding is common with intrathecally delivered ASOs and was considered not responsible for the paralysis of the animal.

Following single escalating intrathecal doses of NVP-13 at dose levels up to 20 mg/animal, plasma and CSF concentrations of NVP-13 generally increased with dose. However, the observed changes in NVP-13 exposure relative to the increases in dose level were inconsistent, probably due to inter-animal variability and the small number of animals (n = 1/sex) used.

Tissue concentrations were measured after final dosing on the day of necropsy (day 36) in kidneys, liver and including spinal cord.

NVP-13 reaches CNS regions of interest following repeated intrathecal administrations with escalating doses.

Phase B: Following single intrathecal doses of NVP-13, at dose levels of 0.8 and 4 mg/animal, the median plasma T_{max} value was 0.5 h at both dose levels. Concentrations declined after T_{max}, but remained above the LLOQ (1.00 ng/mL) at the final sampling time point (24 h after dosing).

Concentrations of NVP-13 in plasma and CSF generally increased with dose level. The observed increases in NVP-13 plasma exposure, as assessed using mean C_{max} and $AUC_{(0–t)}$ values, were dose-proportional.

On Day 14, the highest mean tissue concentrations of NVP-13 were observed in the kidneys. The tissue distribution pattern observed for Day 29 was similar to that on Day 14; however, relatively high levels of NVP-13 were also present in the lumbar spinal cord at both dose levels and in liver at 0.8 mg/animal. The highest mean tissue concentrations

measured for Day 29 represented approximately 30% and 25% of those measured for Day 14, at the 0.8 and 4 mg/animal dose levels, respectively.

Phase C: Following repeated single intrathecal doses of NVP-13, at dose levels of 0.4 and 4 mg/animal/occasion for up to 13 weeks, median T_{max} values in plasma were between 0.5 and 24 h after dosing. Plasma concentrations remained quantifiable at the last sampling time point (24 h after dosing) for all animals on each dosing occasion.

Concentrations of NVP-13 in plasma and CSF increased with dose level. The observed increases in NVP-13 plasma exposure were dose-proportional.

No accumulation of NVP-13 in plasma was observed. Exposure remained consistent throughout the dosing period at the 0.4 mg/animal/occasion dose level, and decreased with increasing number of 4 mg/animal/occasion doses.

For both dose levels, the highest concentrations of NVP-13 in tissues were measured in the lumbar spinal cord and kidney cortex. Mean concentrations in other areas of the brain and in kidney medulla reached NVP-13 levels between approximately 10 and 33% of maximum mean tissue levels, whilst concentrations in the liver represented less than 10% of maximum mean levels.

To assess NVP-13 concentrations within CNS regions, AEX-HPLC analysis was performed in all three phases of the present study. In all phases, NVP-13 was detectable within the main regions of interest, namely the spinal cord (lumbar, thoracic, and cervical), the hippocampus and the subventricular zone (Figure 3A, Figures 5A,B and 10).

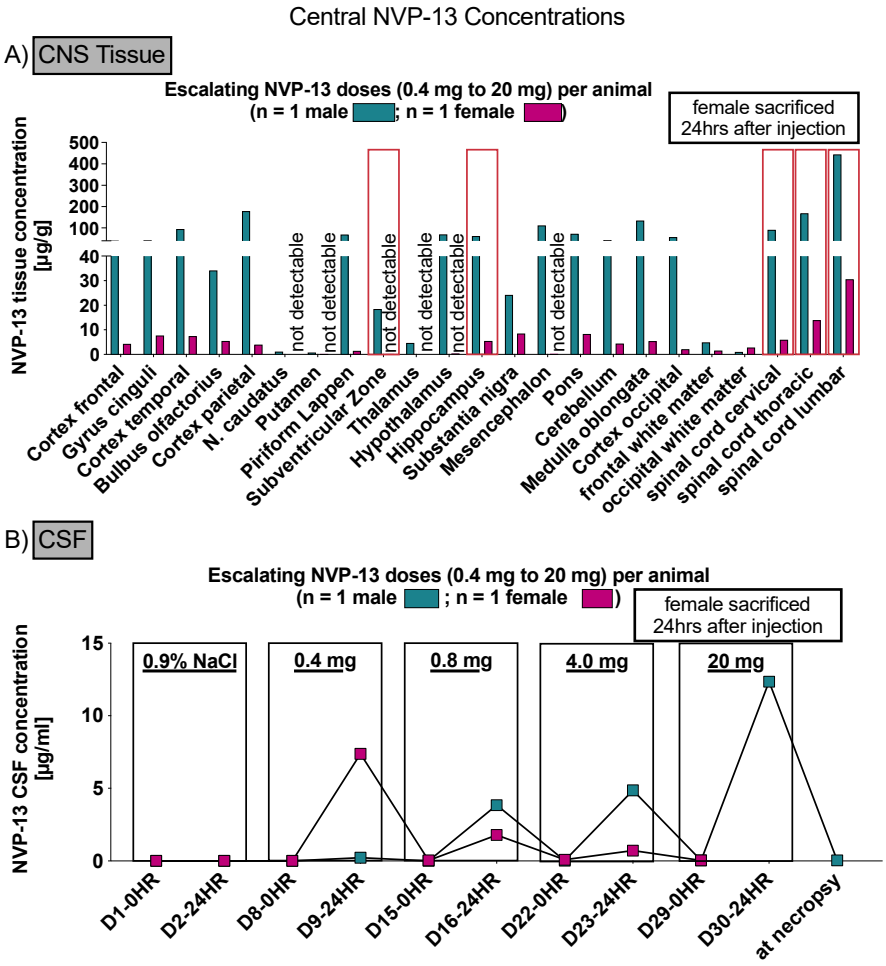

Figure 3. Central NVP-13 tissue concentrations (Phase A). NVP-13 reaches central nervous system regions of interest following repeated intrathecal administrations with escalating doses. The NVP-13 tissue concentrations decreased with increasing distance from the injection side (lumbar spinal cord) (**A**). Further, NVP-13 concentrations were determined within the CSF (**B**).

3.1. NVP-13 Is Detectable within the CSF

To assess NVP-13 concentrations within CSF, AEX-HPLC analysis was performed in all three phases of the present study. In all phases, NVP-13 was detectable within the CSF (Figure 3B, Figures 7 and 12). A summary of gender-averaged toxicokinetic parameters for NVP-13 in CSF is given in Tables 3–6. NVP-13 exerts dose-dependent effects on CSF toxicokinetic parameters in Phase A (Table 3), Phase B (Table 4), and Phase C (Tables 5 and 6).

Table 3. Summary of Gender-Averaged Toxicokinetic Parameters for NVP13 in CSF following Intrathecal Administration to Cynomolgus Monkeys at Escalating Dose Levels—Group 1.

Day	Dose Level (mg/Animal)	C_{max} (ng/mL)	T_{max} (h)	$AUC_{0–24}$ (ng·h/mL)	$AUC_{0–t}$ (ng·h/mL)
8	0.4	309	24.0	NA	NA
15	0.8	6480	24.0	257,000	257,000
22	4.0	13,100	24.0	470,000	470,000
29	20.0	12,300	24.0	458,000	458,000

NA—Not applicable. C_{max} = maximum CSF concentration; T_{max} = time of maximum concentration profile; $AUC_{0–24}$ = area under the CSF concentration-time curve calculated from 0–24 h; $AUC_{0–t}$ = area under the CSF-concentration-time curve calculated from 0–t, where t is the time of the last measurable concentration.

Table 4. Summary of Gender-Averaged Toxicokinetic Parameters for NVP13 in CSF following Single Intrathecal Administrations to Cynomolgus Monkeys Groups 2–5.

Group	Dose Level (mg/Animal)	C_{max} (ng/mL)	T_{max} (h)	$AUC_{0–24}$ (ng·h/mL)	$AUC_{0–t}$ (ng·h/mL)
2–3	0.8	230	24.0	NA	NA
4–5	4.0	689	24.0	NA	NA

NA—Not applicable. C_{max} = maximum CSF concentration; T_{max} = time of maximum concentration profile; $AUC_{0–24}$ = area under the CSF concentration-time curve calculated from 0–24 h; $AUC_{0–t}$ = area under the CSF-concentration-time curve calculated from 0–t, where t is the time of the last measurable concentration.

Table 5. Summary of Gender-Averaged Toxicokinetic Parameters for NVP13 in CSF following Repeated Intrathecal Administration to Cynomolgus Monkeys at a Nominal Dose Level of 0.4 mg/animal/occasion—Group 6.

Day	C_{max} (ng/mL)	T_{max} (h)	$AUC_{0–24}$ (ng·h/mL)	$AUC_{0–t}$ (ng·h/mL)
1	245	42.0	NA	NA
8	405	42.0	NA	24,200
15	2170	24.0	NA	88,800
22	2040	24.0	NA	88,200
29	917	24.0	NA	84,000
43	2880	24.0	NA	201,000
57	1200	21.0	NA	108,000
71	1880	21.0	NA	162,000
85	1510	24.0	NA	667,000

NA—Not applicable. C_{max} = maximum CSF concentration; T_{max} = time of maximum concentration profile; $AUC_{0–24}$ = area under the CSF concentration-time curve calculated from 0–24 h; $AUC_{0–t}$ = area under the CSF-concentration-time curve calculated from 0–t, where t is the time of the last measurable concentration.

3.2. NVP-13 Is Slightly Detectable within Plasma Up to 24 h

To assess NVP-13 concentrations within plasma, AEX-HPLC analysis was performed in all three phases of the present study. In all phases, NVP-13 was detectable within the plasma (Figure 4A, Figures 6 and 11). A summary of gender-averaged toxicokinetic parameters for NVP-13 in plasma is given in Tables 7–10. NVP-13 exerts dose-dependent effects on plasma toxicokinetic parameters in Phase A (Table 7), Phase B (Table 8), and Phase C (Tables 9 and 10).

Table 6. Summary of Gender-Averaged Toxicokinetic Parameters for NVP13 in CSF following Repeated Intrathecal Administration to Cynomolgus Monkeys at a Nominal Dose Level of 4 mg/animal/occasion—Group 7.

Day	C_{max} (ng/mL)	T_{max} (h)	$AUC_{0–24}$ (ng·h/mL)	$AUC_{0–t}$ (ng·h/mL)
1	9830	42.0	NA	NA
8	314	60.0	NA	22,800
15	13,600	21.0	NA	511,000
22	35,700	24.0	NA	1,210,000
29	12,100	24.0	NA	796,000
43	26,500	24.0	NA	1,560,000
57	30,700	63.0	NA	2,060,000
71	22,700	24.0	NA	1,370,000
85	30,400	24.0	NA	1,040,000

NA—Not applicable. C_{max} = maximum CSF concentration; T_{max} = time of maximum concentration profile; $AUC_{0–24}$ = area under the CSF concentration-time curve calculated from 0–24 h; $AUC_{0–t}$ = area under the CSF-concentration-time curve calculated from 0–t, where t is the time of the last measurable concentration.

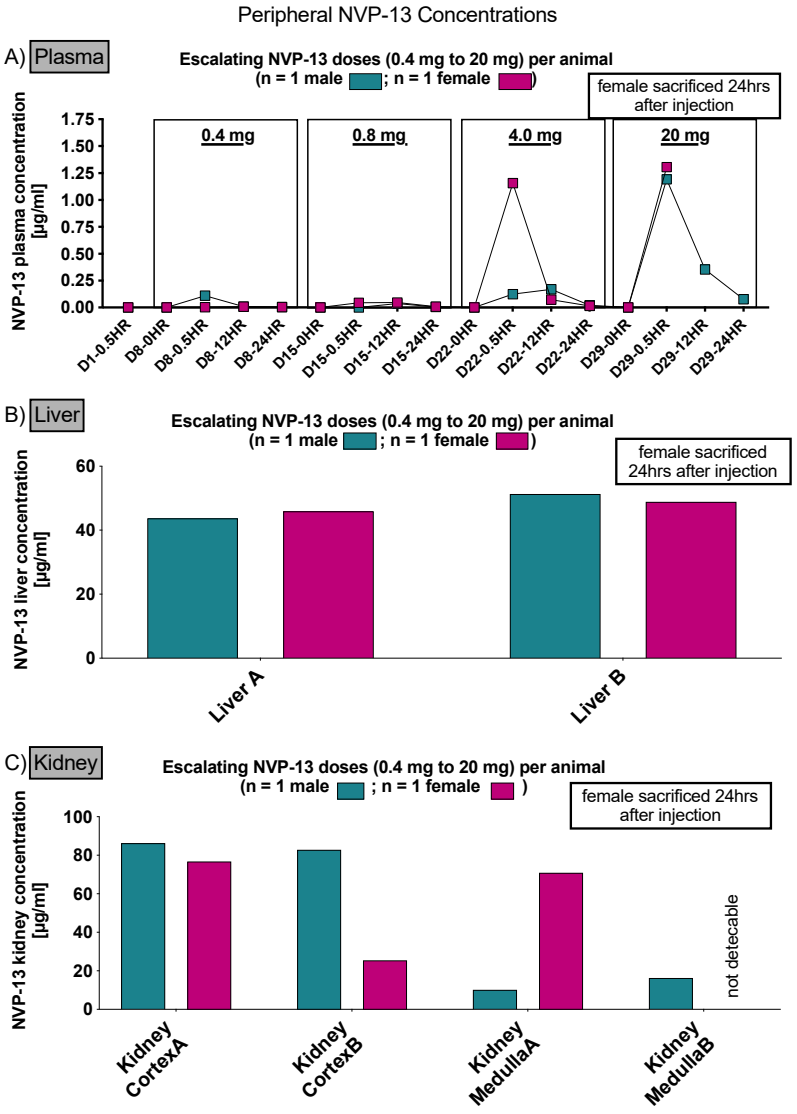

Figure 4. Peripheral NVP-13 tissue concentrations (Phase A). NVP-13 is slightly detectable within plasma samples up to 24 h, with a maximum concentration 0.5 h following intrathecal administration (**A**). Within liver and kidney samples, NVP-13 is also measurable following repeated intrathecal administrations with escalating doses (**B**,**C**).

Table 7. Summary of Gender-Averaged Toxicokinetic Parameters for NVP13 in Plasma following Intrathecal Administration to Cynomolgus Monkeys at Escalating Dose Levels—Group 1.

Day	Dose Level (mg/Animal)	C_{max} (ng/mL)	T_{max} (h)	$AUC_{0–24}$ (ng·h/mL)	$AUC_{0–t}$ (ng·h/mL)
8	0.4	58.6	6.25	343	343
15	0.8	41.7	12.0	788	788
22	4.0	663	6.25	5230	3900
29	20.0	1250	0.500	10,400	10,400

NA—Not applicable; C_{max} = maximum plasma concentration; T_{max} = time of maximum concentration profile; $AUC_{0–24}$ = area under the plasma concentration-time curve calculated from 0–24 h; $AUC_{0–t}$ = area under the plasma-concentration-time curve calculated from 0–t, where t is the time of the last measurable concentration.

Table 8. Summary of Gender-Averaged Toxicokinetic Parameters for NVP13 in Plasma following Single Intrathecal Administrations to Cynomolgus Monkeys—Group 2–5.

Group	Dose Level (mg/Animal)	C_{max} (ng/mL)	T_{max} (h)	$AUC_{0–24}$ (ng·h/mL)	$AUC_{0–t}$ (ng·h/mL)
2–3	0.8	181	0.500	986	986
4–5	4.0	1280	0.500	6040	6040

NA—Not applicable; C_{max} = maximum plasma concentration; T_{max} = time of maximum concentration profile; AUC_{0-24} = area under the plasma concentration-time curve calculated from 0–24 h; $AUC_{0–t}$ = area under the plasma-concentration-time curve calculated from 0–t, where t is the time of the last measurable concentration.

Table 9. Summary of Gender-Averaged Toxicokinetic Parameters for NVP13 in Plasma following Repeated Intrathecal Administration to Cynomolgus Monkeys at a Nominal Dose Level of 0.4 mg/animal/occasion—Group 6.

Day	C_{max} (ng/mL)	T_{max} (h)	$AUC_{0–24}$ (ng·h/mL)	$AUC_{0–t}$ (ng·h/mL)
1	63.7	1.94	396	396
8	158	0.500	630	630
15	42.5	7.69	308	308
22	26.6	3.38	219	219
29	26.4	4.81	225	225
43	93.2	7.69	184	184
57	48.0	4.81	334	334
71	46.0	7.69	NA	510
85	37.6	9.13	NA	609

NA—Not applicable; C_{max} = maximum plasma concentration; T_{max} = time of maximum concentration profile; $AUC_{0–24}$ = area under the plasma concentration-time curve calculated from 0–24 h; $AUC_{0–t}$ = area under the plasma-concentration-time curve calculated from 0–t, where t is the time of the last measurable concentration.

Table 10. Summary of Gender-Averaged Toxicokinetic Parameters for NVP13 in Plasma following Repeated Intrathecal Administration to Cynomolgus Monkeys at a Nominal Dose Level of 4 mg/animal/occasion—Group 7.

Day	C_{max} (ng/mL)	T_{max} (h)	$AUC_{0–24}$ (ng·h/mL)	$AUC_{0–t}$ (ng·h/mL)
1	1330	0.500	NA	5870
8	2240	0.500	NA	7590
15	580	1.94	NA	3480
22	882	4.81	NA	4220
29	827	6.25	NA	3830
43	436	3.38	NA	3120
57	310	6.25	NA	2360
71	314	4.81	NA	2510
85	178	9.13	NA	2160

NA—Not applicable; C_{max} = maximum plasma concentration; T_{max} = time of maximum concentration profile; $AUC_{0–24}$ = area under the plasma concentration-time curve calculated from 0–24 h; $AUC_{0–t}$ = area under the plasma-concentration-time curve calculated from 0–t, where t is the time of the last measurable concentration.

As already stated above, in order to assess NVP-13 concentrations within CNS regions, AEX-HPLC analysis was performed and NVP-13 was detectable within the main regions of interest, namely the spinal cord (lumbar, thoracic, and cervical), the hippocampus and the subventricular zone (Figure 5A,B) following one single i.th administration, on day 15 and day 29.

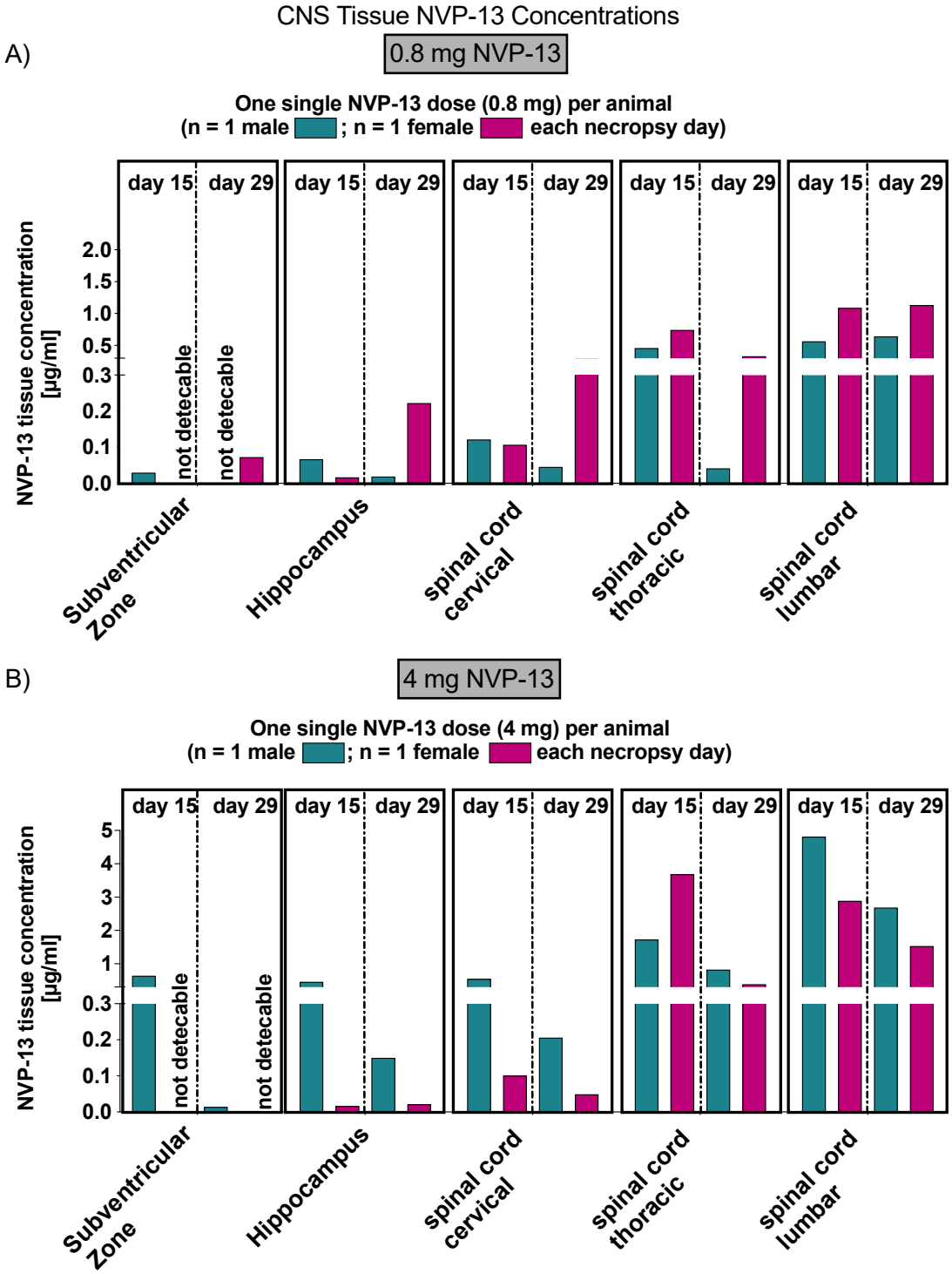

Figure 5. Central NVP-13 tissue concentrations (Phase B). NVP-13 reaches central nervous system regions of interest following single intrathecal administrations with two different doses, respectively (**A**,**B**). Tissues levels depended on the dose administered. Again, the tissue concentrations decreased with increasing distance from the injection side (lumbar spinal cord).

Similar to phase A, NVP-13 concentrations were assessed within CNS regions by AEX-HPLC analysis. NVP-13 was detectable within the CSF and plasma (Figures 6 and 7) following one single i.th administration, on day 15 and day 29.

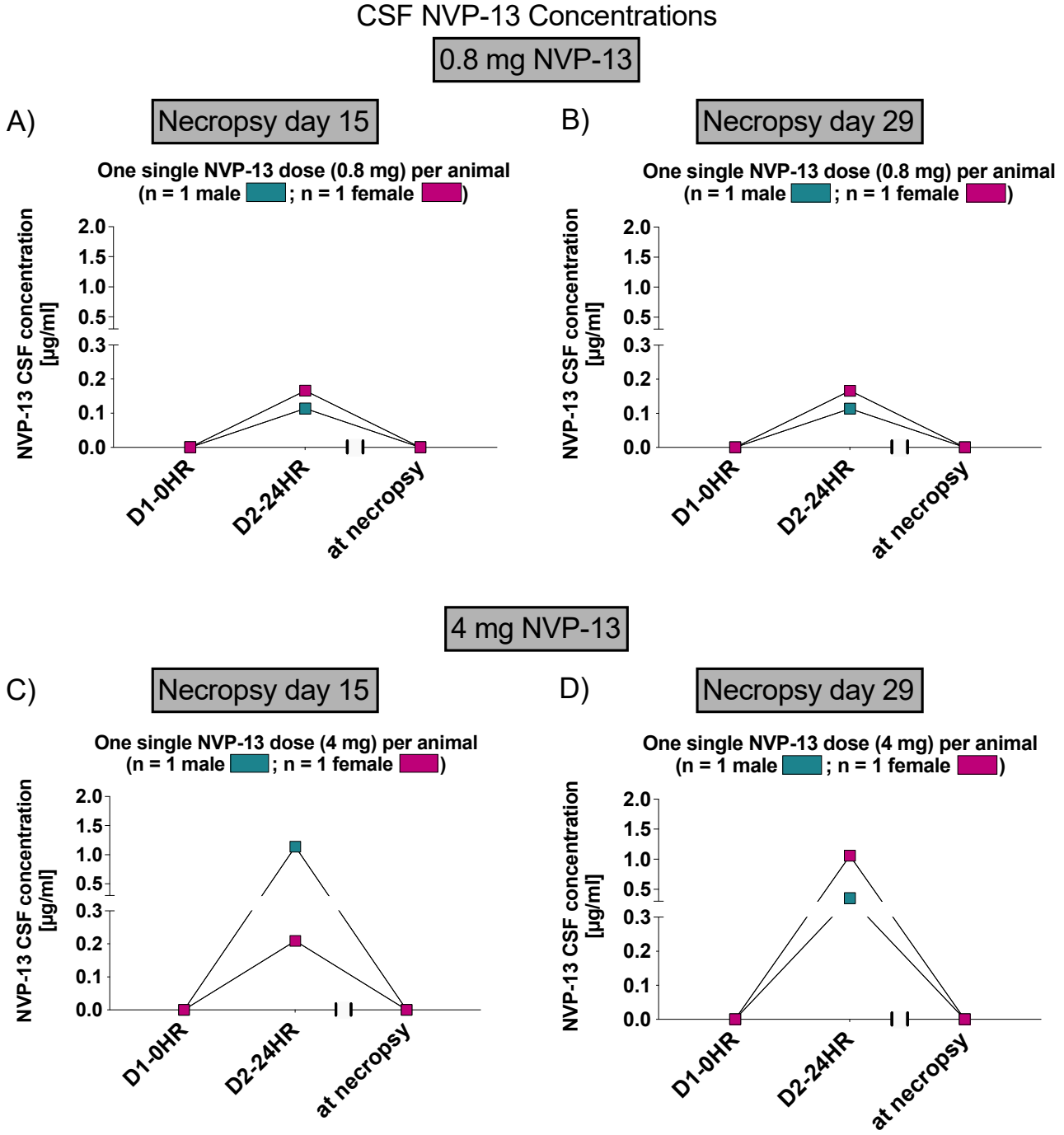

Figure 6. CSF NVP-13 concentrations (Phase B). NVP-13 concentrations are detectable within the CSF in a dose-dependent manner 24 h following one single intrathecal administration (**A**–**D**).

Again, to assess NVP-13 concentrations within peripheral tissue (liver and kidney), AEX-HPLC analysis was performed and, NVP-13 was detectable (Figures 8 and 9), on day 15 and 29.

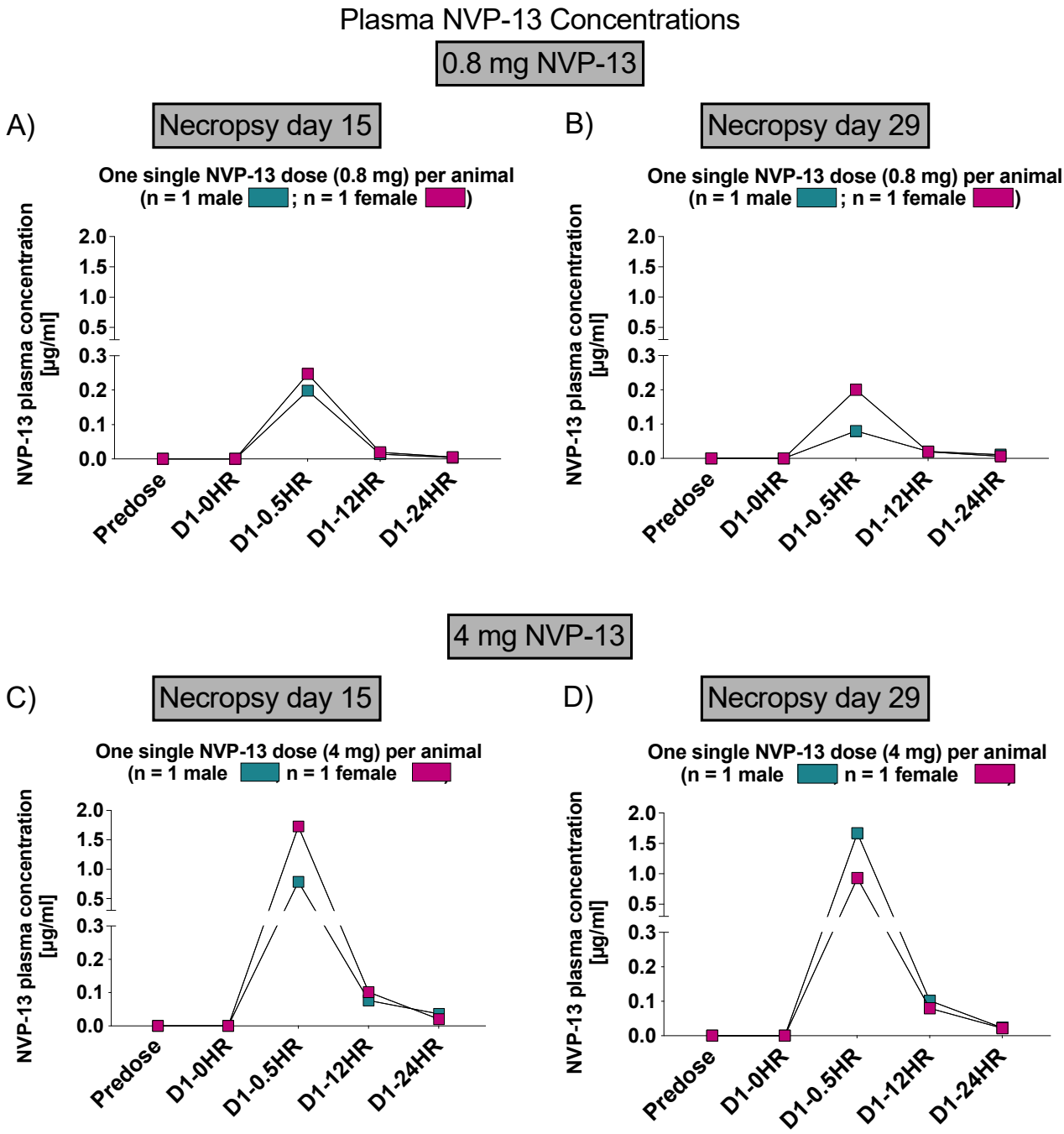

Figure 7. Plasma NVP-13 concentrations (Phase B). Within plasma samples, NVP-13 is slightly detectable up to 24 h and in a dose-dependent manner. Plasma levels depended on the dose administered with a maximum concentration 0.5 h following the dosing procedure (**A**–**D**).

Similar to phase A and B, NVP-13 concentrations within CNS regions of interest were determined by AEX-HPLC analysis.. Again, NVP-13 was detectable in all areas on day 91 of the experiment (Figure 10)

Similar to phase A and B, NVP-13 concentrations within CSF and plasma were determined by AEX-HPLC analysis (Figures 11 and 12).

Finally, NVP-13 concentrations were also detectable in peripheral tissues (liver and kidney) in phase C on day 91 of the experiment (Figure 13).

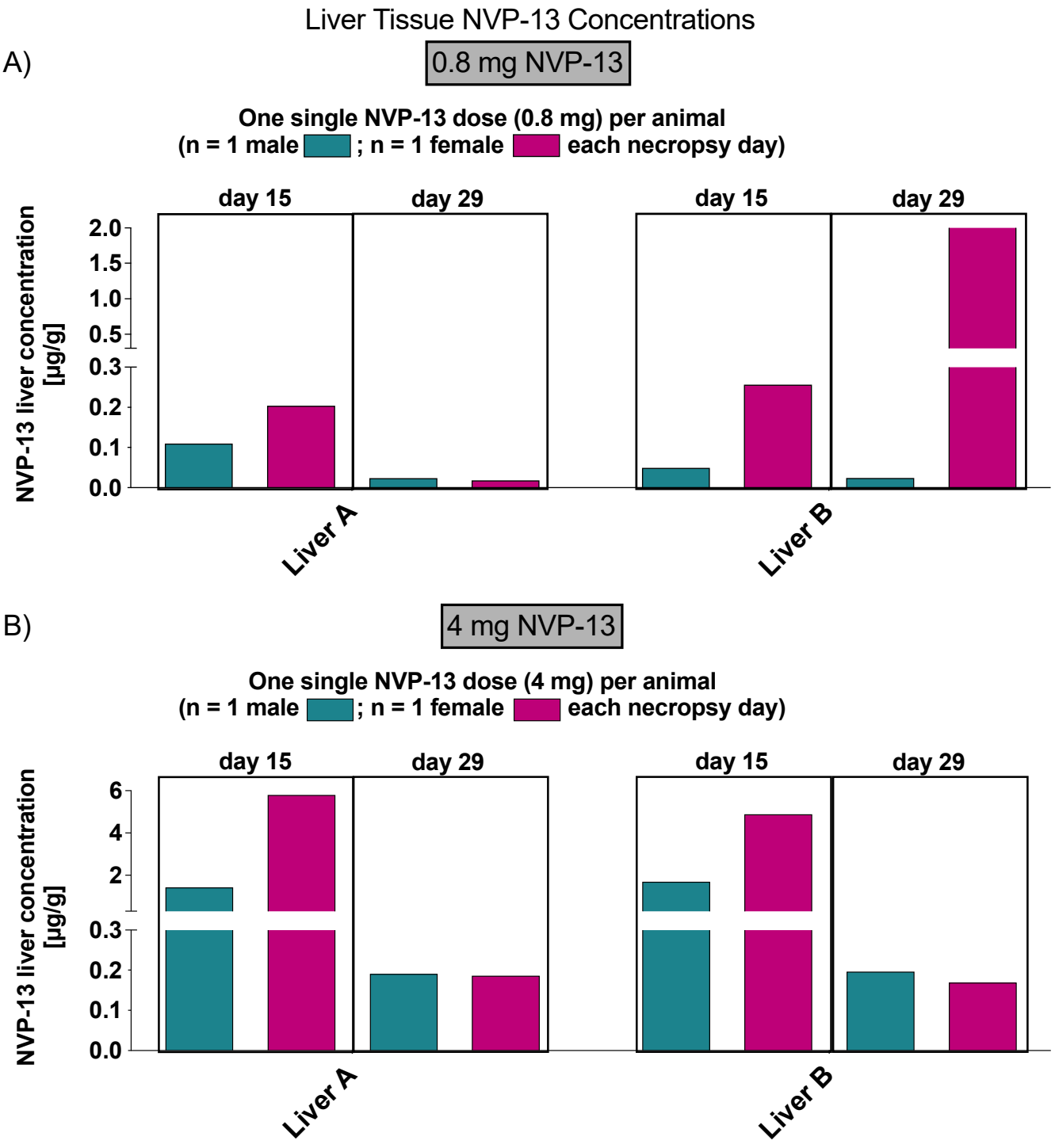

Figure 8. NVP-13 liver tissue concentrations (Phase B). NVP-13 is detectable within liver samples in a dose-dependent manner, in both 15 (**A**) and 29 (**B**) days following intrathecal administration.

3.3. Effects of NVP-13 on Physiological Parameters

To assess effects of repeated NVP-13 administrations on standard in-life parameters (behavior and appearance, feces, morbidity and mortality, and body weight development, data (not shown) were monitored throughout the entire experiment (for details, see study plan). For none of the three read-out parameters, any unusual changes were noted.

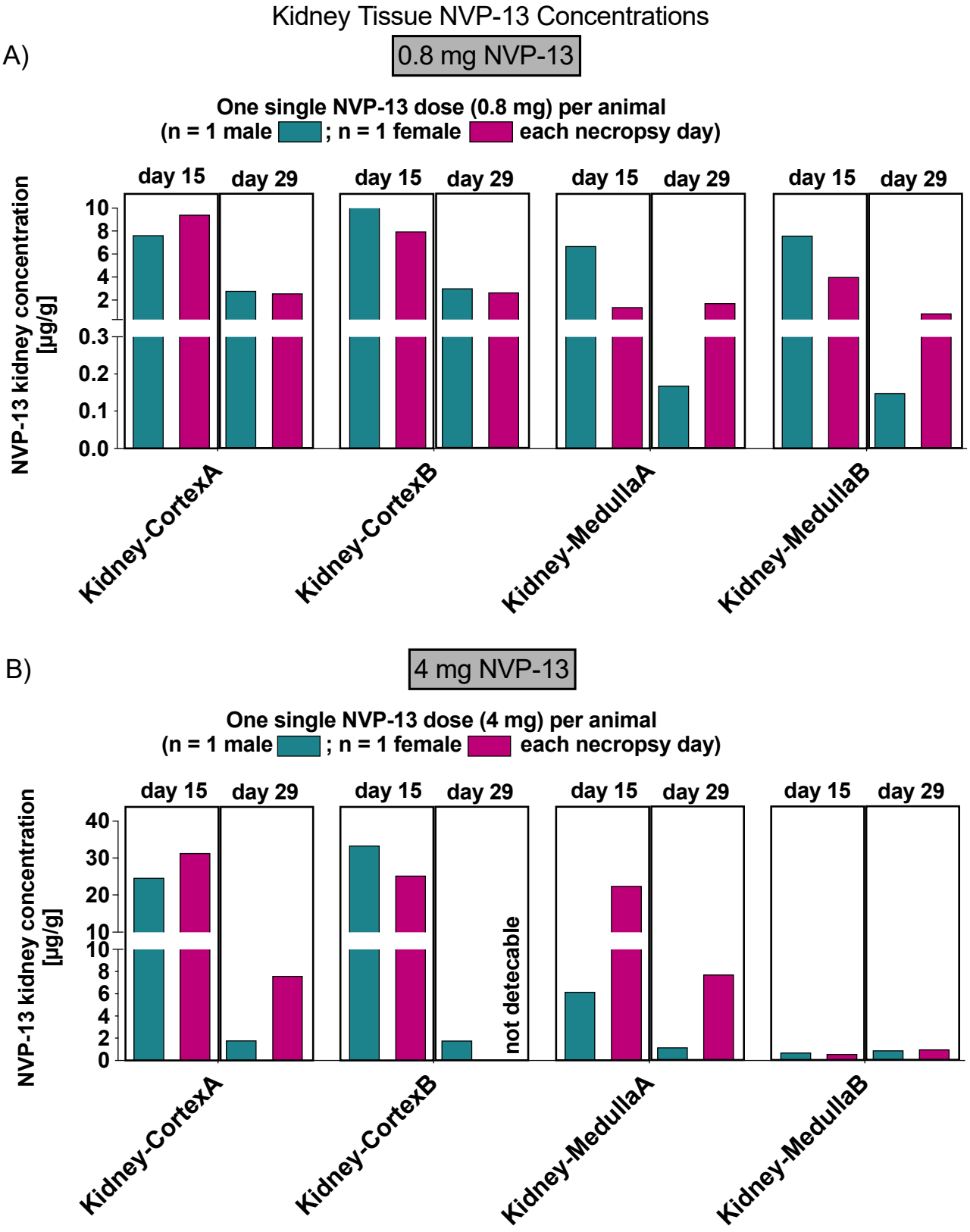

Figure 9. NVP-13 kidney tissue concentrations (Phase B). NVP-13 is detectable within kidney samples (cortex and medulla) in a dose-dependent manner, in both 15 (**A**) and 29 (**B**) days following intrathecal administration.

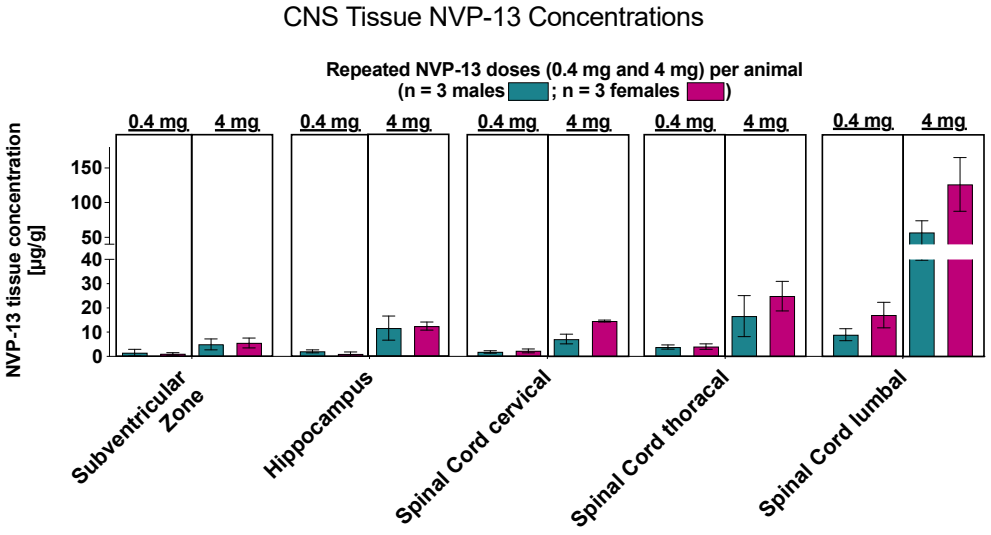

Figure 10. Central NVP-13 tissue concentrations (Phase C). NVP-13 reaches central nervous system regions of interest following repeated intrathecal administrations with escalating doses. Again, the tissue concentrations decreased with increasing distance from the injection side.

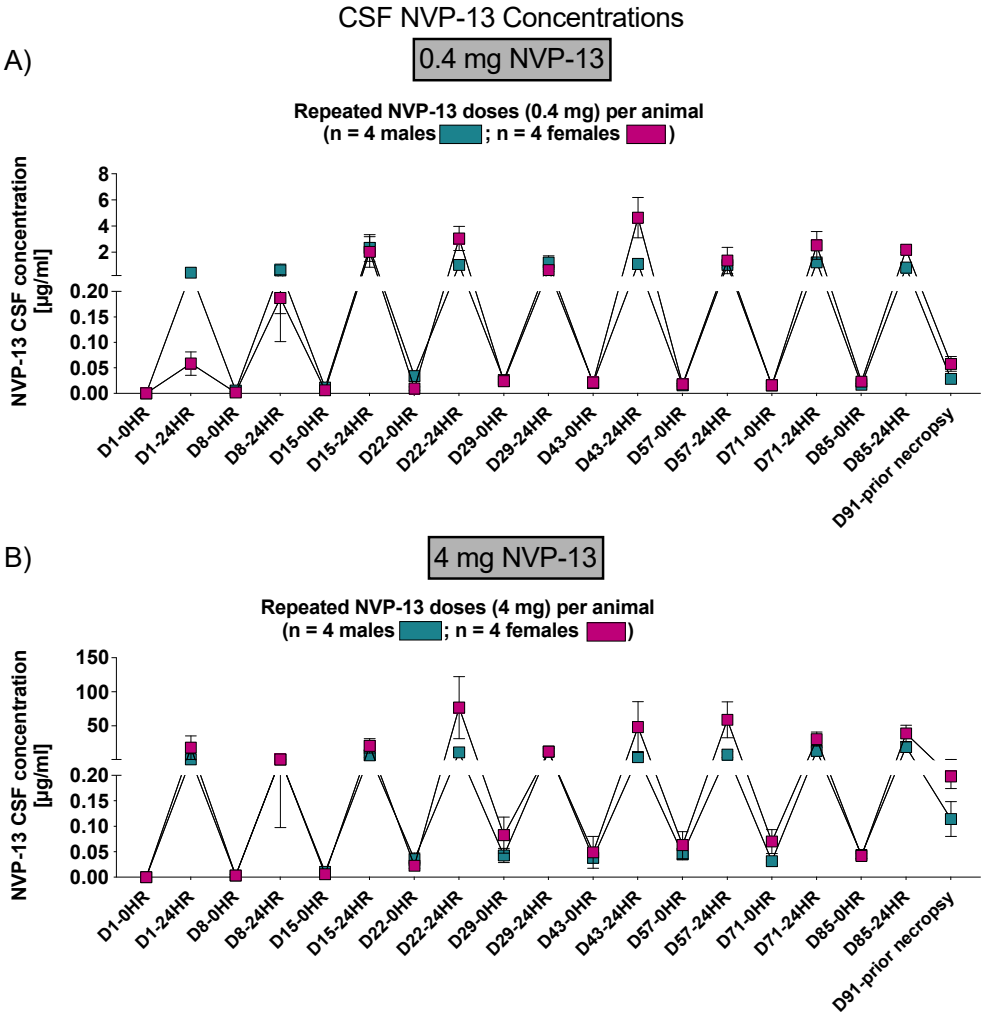

Figure 11. CSF NVP-13 concentrations (Phase C). NVP-13 concentrations were detectable within the CSF following 24 h of intrathecal administrations in a dose-dependent manner and treatment-relevant dose range (**A**,**B**).

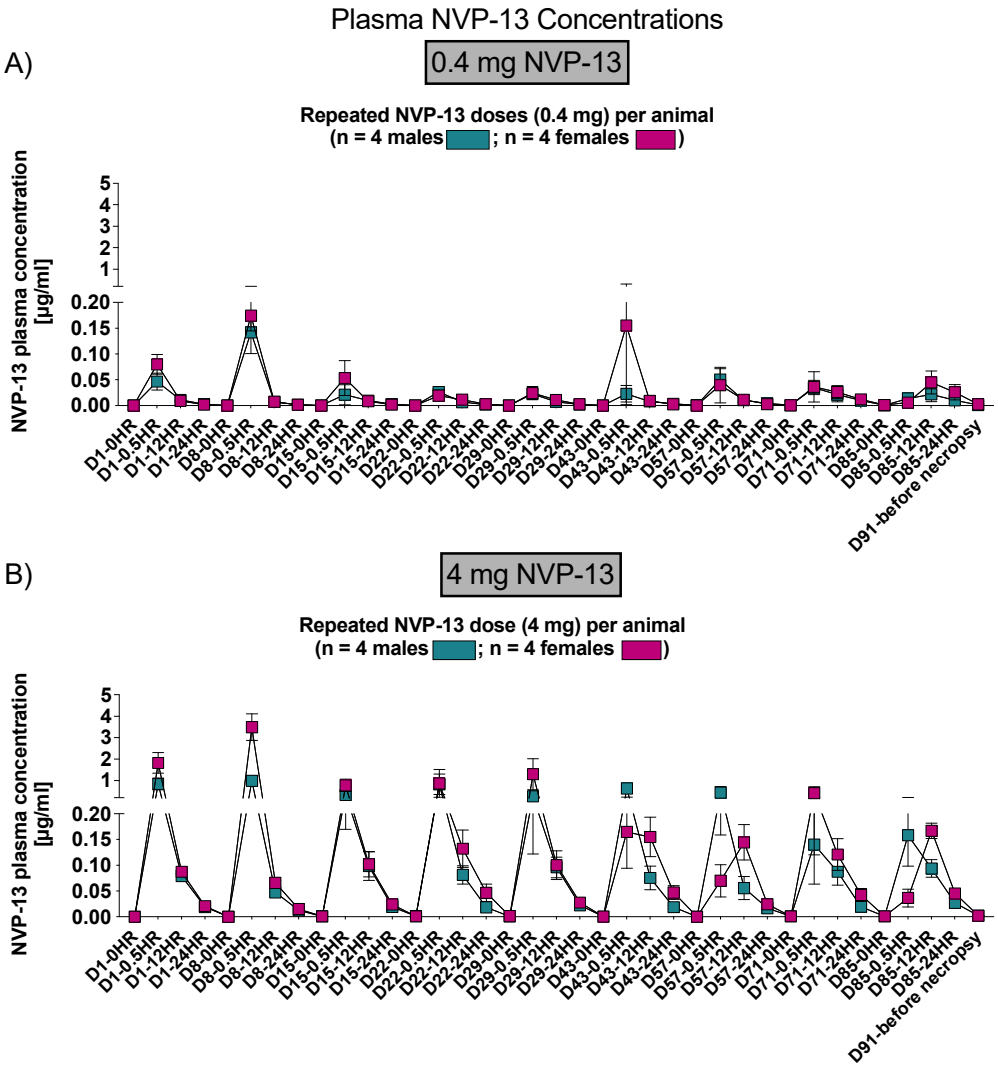

Figure 12. Plasma NVP-13 tissue concentrations (Phase C). NVP-13 concentrations were detectable within the plasma following 12 h (0.4 mg/animal) and following 24 h (4 mg/animal) of intrathecal administrations in a dose-dependent manner and treatment-relevant dose range (**A**,**B**).

3.4. Effects of NVP-13 on Physical Parameters

To assess effects of repeated NVP-13 administrations on physical parameters, physical examinations were performed on all unsedated animals throughout the entire experiment (for details, see study plan). During Phase A, only the high dose of 20 mg/animal resulted in paralysis of the arms and legs; these findings led to the premature sacrifice of this animal, which indicated the dose level was above the maximum tolerated dose.

Physical examinations during Phase B did not show any post-dose absence of reflexes in animals administered 0.4 or 4.0 mg/animal.

During Phase C, all but one animal administered 0.4 g/animal (Animal P0604; Group 6) were observed with a regain of lower abdominal reflex losses after a maximum of 48 h. However, Animal P0604 was also not showing an adverse test item-related reflex loss, as the patellar reflex on both sides was already absent before dose initiation.

3.5. Effects of NVP-13 on Neurobehavioral Parameters

To assess effects of repeated NVP-13 administrations on neurobehavioral parameters, a standard observation sequence, which allowed the assessment of peripheral and central nervous system activities, using a modified version of primary observation test described by

Irwin for detecting neurological and behavioral tests in mice (Irwin, 1968), was performed. Here, no adverse or test item-related findings were noted.

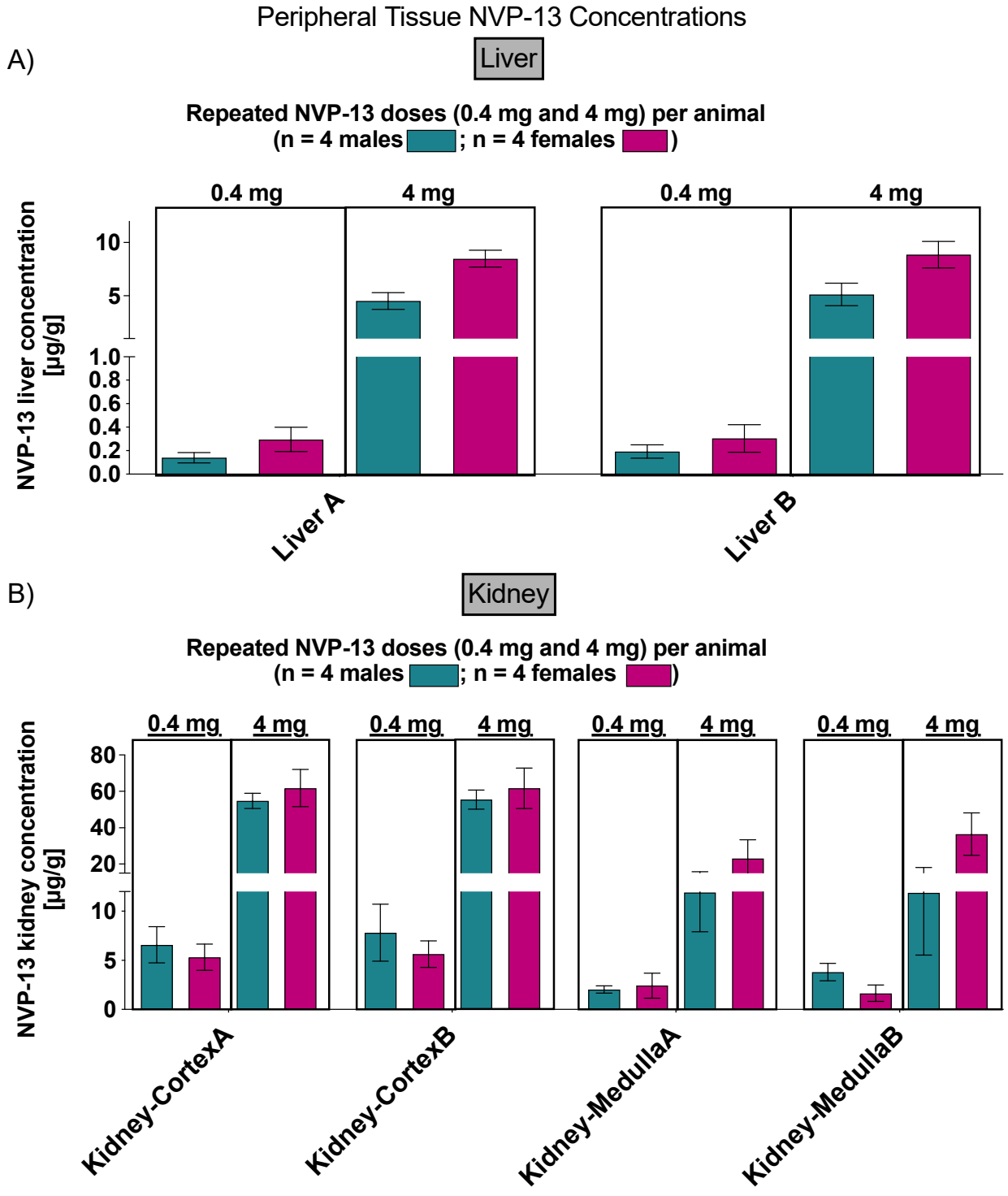

Figure 13. Peripheral NVP-13 tissue concentrations (Phase C). NVP-13 is detectable within liver (**A**) and kidney (cortex and medulla) (**B**) samples in a dose-dependent manner.

3.6. Effects of NVP-13 on Neurological Parameters

To assess effects of repeated NVP-13 administrations on physical parameters, physical examinations were performed on animals without further medication throughout the entire

experiment (for details, see study plan). Here, no adverse or test item-related findings were noted.

3.7. Effects of NVP-13 on Ophthalmic Parameters

To assess effects of repeated NVP-13 administrations on ophthalmic parameters, animals were anesthetized with ketamine and medotomidine, and a mydriatic agent (1% tropicamide) was instilled into eyes prior to examination. Atipamezole was used as an antidote at the end of the investigation. All investigations were performed on all animals throughout the entire experiment (for details, see study plan). Macroscopic examinations were performed on eye and periocular tissues. The ocular fundus, with macula lutea, papilla, ocular vessels, and retina were examined. Anterior and medium segments, with conjunctiva, cornea, anterior chamber, iris, lens, and vitreous body, were examined by slit-lamp microscopic. Fluorescein was instilled onto the cornea for epithelial staining. For none of these parameters, an adverse or test item-related findings were noted

3.8. Effects of NVP-13 on Hematological Parameters

To assess effects of repeated NVP-13 administrations on hematological parameters, blood samples were withdrawn and analyzed from all animals throughout the entire experiment (for details, see study plan). For none of the measured parameters, any adverse or test item-related changes were noted.

3.9. Effects of NVP-13 on Coagulation

To assess effects of repeated NVP-13 administrations on coagulation, Prothombin Time (PT.) and Activated Partial Thromboplastin Time (APTT.) were determined from blood collected into trisodium citrate anticoagulant. For none of the 2 parameters, any adverse or test item-related changes were noted.

3.10. Effects of NVP-13 on Clinical Chemistry

To assess effects of repeated NVP-13 administrations on clinical chemistry, respective parameters were analyzed (for details, see study plan). For none of the measured parameters, any adverse or test item-related changes were noted.

3.11. Effects of NVP-13 on Histology

To assess effects of repeated NVP-13 administrations on histology (Table 11), tissues from each animal were trimmed and embedded in paraffin wax, sectioned at a nominal 5 µm, and stained with hematoxylin and eosin. All differences between test item-treated groups and controls were interpreted as incidental (for instance, differences in sexual organ weights) and/or within normal range of variation because they were present only in absolute weight or in relative (to body or brain weight) ratio, they lacked a histological correlate, or the difference was very small.

Macroscopic Observations: The only macroscopic observation described in the present study, namely a marked autolysis, arose in one female animal (Phase A) following 20-mg NVP-13 i.th administration. No other macroscopic findings due to NVP-13 administrations were noted in Phase B, or C.

Microscopic Observations: Test item-related changes were observed in the central nervous system (including the IT injection site). These changes occurred at all dose levels, with no dose relationship.

Central Nervous System: Hippocampal vacuoles have been described as a fixation artefact related to the cellular uptake of ASOs and the subsequent washout during tissue processing for microscopic evaluation [31]. In this study, similar neuronal vacuolation was noted in the unscheduled sacrifice animal (Animal P0101F), and after five escalating doses (0.4, 0.8, 4, and 20 mg/animal) over 29 days and in two animals, after nine doses of 4 mg/animal over 13 weeks.

Table 11. Incidence and severity of NVP-13-related microscopic findings in Phase C. Repeated intrathecal NVP-13 administration for 13 consecutive weeks (Phase C) resulted in minimal to slight microscopic dose-independent alterations withing central nervous tissue.

Sex	NVP13			
	Males		Females	
Dose Level (mg/animal)	0.4	4.0	0.4	4.0
Number Examined	4	4	4	4
Brain				
Vacuoles, neuron				
Minimal	0	1	0	1
Infiltrate, mononuclear cells				
Minimal	3	2	2	4
Slight	1	2	2	0
Perivascular cuff				
Minimal	0	2	1	0
Slight	0	0	1	0
Edema, meninges				
Minimal	3	3	2	2
Slight	1	1	2	1
Gliosis				
Minimal	0	0	1	1
Spinal cord, cervical				
Infiltrate, mononuclear cells				
Minimal	2	3	3	1
Slight	1	0	0	0
Spinal cord, thoracic				
Infiltrate, mononuclear cells				
Minimal	2	3	2	2
Slight	0	0	0	1
Spinal cord, lumbar				
Infiltrate, mononuclear cells				
Minimal	3	1	2	2
Slight	1	2	1	2
Inflammation, subacute; dura				
Slight	1	1	1	0
Intrathecal Injection Site				
Infiltrate, mononuclear cells				
Minimal	2	2	2	4
Slight	2	2	2	0
Inflammation, subacute; dura				
Slight	0	2	2	1

During all phases and at all doses, infiltrates of mononuclear cells were noted in the brain (frequently accompanied by perivascular cuffs), spinal cord, intrathecal injection site, and spinal nerve roots of animals, and meningeal oedema was noted in the brain; these findings were considered test item-related and consequences of the mild proinflammatory effect described for ASOs (e.g., vasculitis/inflammatory infiltrates) [32]. Only in Phase C, mononuclear cell infiltrates were found in the dura mater of the spinal cord lumbar and intrathecal injection site, indicating a dose-dependent increase of this inflammatory reaction.

In the thoracic and lumbar parts of the spinal cord, minimal to slight white matter vacuolation was found sporadically; this finding was considered related to the slight traumatic event induced by intrathecal injection procedures in the lumbar region, as frequently observed in controls following intrathecal application.

4. Discussion

The concept of the present study has been successfully applied to support first-in-human clinical trials and has found acceptance by regulatory bodies (BfArM in Germany).

The entire non-GLP program was completed within less than 6 months and represents a valuable blueprint for fast-track development of oligonucleotides. Furthermore, applying the described concept will result in using fewer animals in comparison to the conduct of three independent studies (maximum tolerated dose study, pharmacokinetic and biodistribution study, and repeated dose-range-finding study). As we move forward with ASO-based therapies [5], the design and conduct of non-human primate studies will require constant review and improvement, as, in comparison to classical small molecules and biologics, comparison data are utmost limited.

By measuring ASO concentrations within CNS tissue, CSF, peripheral tissue, and plasma, physiological and physical, neurobehavioral and neurological, but also hematological and clinical chemistry parameters, this study paradigm gives a good characterization profile of the respective test compound.

Due to the inability of ASO crossing the blood brain barrier on the one hand and the need for central ASO concentrations to treat neurodegenerative disorders, an intrathecal administration was performed as described in other studies [4]. In vivo NVP-13 i.th. administrations led to dose-dependent ASO concentrations within CNS tissue. Hereby, dose levels indirectly correlated with distance to the respective area of injection, the lumbar spinal cord, which is in line with previous studies in mice, juvenile cynomolgus monkeys, human infants, and own in vivo data (Peters et al., Pharmaceutics, under review). Within the CNS, ASOs are well distributed by intrinsic CSF dynamics. For details, see Bennett et al., 2019 [4].

NVP-13 levels were also detectable in peripheral organs, namely the kidney and the liver, at treatment active drug levels, but also indicating the regular physiological way of substance distribution and decay. Calculation for gender ratios (male/female) indicated sex differences in the toxicokinetics of NVP-13 following i.th administration. Further, concentration-time profiles show a general enhancement of NVP-13 levels with increasing dose levels for all three phases.

The only macroscopic observation described in the present study, namely a marked autolysis, arose in one female animal (phase A) following 20 mg NVP-13 i.th administration. This indicates an enhanced enzymatic digestion of cells by the action of its own enzymes and occurs mostly in dying or even dead cells [33] and might be an explanation for the impaired neurological behavior (paralysis of arms and legs) in this animal as a direct result of the i.th. injection. A second explanation might be a test item-related change in vacuoles in the neuronal cell bodies. Here, minimal, multifocal, neuronal vacuoles (clear and empty) were found in the hippocampus (affecting CA1 area of the cornu ammonis) and cerebral cortex. A refutation for the influence of these vacuoles on neurological behavior is described by Engelhardt et al. Here, comparable vacuoles have been described as a fixation artefact related to the cellular uptake of ASOs and the subsequent washout during tissue processing for microscopic evaluation [31]. The presence of comparable vacuoles in male and female animals out of Phase C (Table 11) give further evidence for no direct effect on neurological parameters. Finally, a high concentration of ions surrounding spinal rout ganglions following the high NVP-13 dose or a compression as a result of the i.th. administration process might have led to the neurological behavior.

The test item-related inflammatory reactions (mononuclear cell infiltrates, perivascular cuffs) were noted in the meninges of the brain (cerebral cortex, sporadically cerebellum) and spinal cord (cervical, thoracic, and lumbar; dura mater of spinal cord), adjacent to the intrathecal injection site (lumbar spinal cord), in the spinal nerve roots, and adjacent to the intrathecal injection site of most animals during all phases and all doses. In Phase C only, mononuclear cell infiltrates were found in the dura mater of the spinal cord lumbar and intrathecal injection site, indicating a dose-dependent increase of this inflammatory reaction (Table 11). During all phases and at all doses, infiltrates of mononuclear cells were noted in the brain (frequently accompanied by perivascular cuffs), spinal cord, intrathecal injection site, and spinal nerve roots of animals, and meningeal edema was noted in the brain; these findings were considered test item-related and consequences of the mild

proinflammatory effect described for ASOs (e.g., vasculitis/inflammatory infiltrates) [32]. In addition to the mononuclear cell infiltrates observed in the current study, splenomegaly and lymphoid hyperplasia are well-known subchronic toxicity effects. This non-specific immune stimulation is due to an unmethylated cytosine-phosphorous-guanine (CpG) motif in the ASO sequence which is recognized by Toll-like receptor -9 immune cells. Following activation, proinflammatory cytokines including IL-6, IL-12, and INF-gamma are released and B-cell proliferation, antibody production as well as T-lymphocyte and natural killer cell activation is promoted [26,34]. In terms of no severe physiological, neurological, and neurobehavioral observations, except the female in Phase A, observed in this approach, the effects of NVP-13 on immunity are considered as non-adverse, which is in line with the safe and low toxic drug profile of a broad variety of ASOs for the treatment of different disorders.

5. Conclusions

In conclusion, we were able to design a highly innovative approach to assess toxicity and pharmacokinetics for antisense oligonucleotides in Cynomolgus monkeys, in general, and for NVP-13, in particular. Taken together, the results of the current study indicate that the novel LNA Gapmer ASO NVP-13 is well-tolerated up to 4.0 mg/dose and shows the expected pharmacokinetic profile of an i.th. administered ASO. Therefore, the 4.0 mg/dose results in a comfortable probable high-dose level for a subsequent GLP repeated-dose toxicity study. However, this dose level did not thereby become a mandatory dose in the GLP study, but rather defined the verified upper possible end.

Author Contributions: Conceptualization, S.P., S.K. (Sven Korte), L.M., T.-H.B. and U.B.; data curation, S.P.; formal analysis, S.P., S.K. (Sven Korte), T.-H.B. and U.B.; funding acquisition, T.-H.B. and U.B.; investigation, S.P., E.W., S.K. (Sabrina Kuespert), R.H., S.K. (Sven Korte), L.M., S.J., T.-H.B. and U.B.; methodology, S.P., E.W., S.K. (Sabrina Kuespert), R.H., S.K. (Sven Korte), L.M., L.A., S.J., T.-H.B. and U.B.; project administration, T.-H.B. and U.B.; supervision, T.-H.B.; validation, U.B.; writing—original draft, S.P.; writing—review and editing, E.W., S.K. (Sabrina Kuespert), R.H., S.K. (Sven Korte), L.M., L.A., S.J., T.-H.B. and U.B. All authors have read and agreed to the published version of the manuscript.

Funding: This study was funded by the German Federal Ministry of Education and Research (BMBF, Project GO-Bio: 031A386, MND-Net), the German Ministry of Economics and Energy (BMWI, ZIM-funding: KF2525608MD3) and the Bavarian Ministry of Economics, Energy and Infrastructure (PTJ, BayBIO: BIO-1506-0002). The authors are grateful to the German First-Bundesliga Team RB Leipzig for their generous ALS-Research donation.

Institutional Review Board Statement: This study was performed in compliance with the following guidelines or recommendations concerning preclinical development of human pharmaceuticals: European Directive 2001/83/EC and all subsequent amendments; German Drug Law; International Conference on Harmonization (ICH) Guideline: Guidance on Non-clinical Safety Studies for the Conduct of Human Clinical Trials and Marketing Authorization for Pharmaceuticals, M3(R2), issued in EMA as CPMP/ICH/286/95.

Data Availability Statement: The authors declare that (the/all other) data supporting the findings of this study are available within the paper. Additional information/data on NVP-13 that support the findings of this study are available from the corresponding author upon reasonable request.

Acknowledgments: The authors are grateful to U. Fink and J. Strey (both Projektträger Jülich, PTJ) for great advisory support. We are very grateful to Ulrich Granzer and his team, especially to Anita Friedrich and Susanne Mailänder, for outstanding advice and continuous support.

Conflicts of Interest: U.B. and L.A. hold intellectual property on TGF-beta receptor modulators. All other authors declare that they do not have any conflict of interest.

References

1. Zamecnik, P.C.; Stephenson, M.L. Inhibition of Rous sarcoma virus replication and cell transformation by a specific oligodeoxynucleotide. *Proc. Natl. Acad. Sci. USA* **1978**, *75*, 280–284. [CrossRef]
2. Stephenson, M.L.; Zamecnik, P.C. Inhibition of Rous sarcoma viral RNA translation by a specific oligodeoxyribonucleotide. *Proc. Natl. Acad. Sci. USA* **1978**, *75*, 285–288. [CrossRef]
3. DeVos, S.L.; Miller, T.M. Antisense oligonucleotides: Treating neurodegeneration at the level of RNA. *Neurotherapeutics* **2013**, *10*, 486–497. [CrossRef] [PubMed]
4. Bennett, C.F.; Krainer, A.R.; Cleveland, D.W. Antisense Oligonucleotide Therapies for Neurodegenerative Diseases. *Annu. Rev. Neurosci.* **2019**, *42*, 385–406. [CrossRef] [PubMed]
5. Crooke, S.T.; Baker, B.F.; Crooke, R.M.; Liang, X.-H. Antisense technology: An overview and prospectus. *Nat. Rev. Drug Discov.* **2021**, *20*, 427–453. [CrossRef] [PubMed]
6. Chiriboga, C.A.; Swoboda, K.J.; Darras, B.T.; Iannaccone, S.T.; Montes, J.; De Vivo, D.C.; Norris, D.A.; Bennett, C.F.; Bishop, K.M. Results from a phase 1 study of nusinersen (ISIS-SMN Rx) in children with spinal muscular atrophy. *Neurology* **2016**, *86*, 890–897. [CrossRef]
7. Haché, M.; Swoboda, K.J.; Sethna, N.; Farrow-Gillespie, A.; Khandji, A.; Xia, S.; Bishop, K.M. Intrathecal Injections in Children with Spinal Muscular Atrophy. *J. Child Neurol.* **2016**, *31*, 899–906. [CrossRef]
8. Wurster, C.D. Intrathecal administration of nusinersen in adolescent and adult SMA type 2 and 3 patients. *J. Neurol.* **2019**, *266*, 183–194. [CrossRef]
9. Neil, E.E.; Bisaccia, E.K. Nusinersen: A Novel Antisense Oligonucleotide for the Treatment of Spinal Muscular Atrophy. *J. Pediatric Pharmacol. Ther.* **2019**, *24*, 194–203. [CrossRef]
10. Kandasamy, M.; Aigner, L. Neuroplasticity, limbic neuroblastosis and neuro-regenerative disorders. *Neural Regen Res.* **2018**, *13*, 1322–1325. [CrossRef]
11. Kandasamy, M.; Rosskopf, M.; Wagner, K.; Klein, B.; Couillard-Despres, S.; Reitsamer, H.A.; Stephan, M.; Nguyen, H.P.; Riess, O.; Bogdahn, U.; et al. Reduction in Subventricular Zone-Derived Olfactory Bulb Neurogenesis in a Rat Model of Huntington's Disease Is Accompanied by Striatal Invasion of Neuroblasts. *PLoS ONE* **2015**, *10*, e0116069. [CrossRef]
12. Winner, B.; Winkler, J. Adult Neurogenesis in Neurodegenerative Diseases. *Cold Spring Harb. Perspect. Biol.* **2015**, *7*, a021287. [CrossRef] [PubMed]
13. Gómez-Pinedo, U. Notch Signalling in the Hippocampus of Patients with Motor Neuron Disease. *Front. Neurosci.* **2019**, *13*, 302. [CrossRef] [PubMed]
14. Peters, S.; Zitzelsperger, E.; Kuespert, S.; Iberl, S.; Heydn, R.; Johannesen, S.; Petri, S.; Aigner, L.; Thal, D.R.; Hermann, A.; et al. The TGF-β System as a Potential Pathogenic Player in Disease Modulation of Amyotrophic Lateral Sclerosis. *Front. Neurol.* **2017**, *8*, 669. [CrossRef]
15. Fakhoury, M. Immune-mediated processes in neurodegeneration: Where do we stand? *J. Neurol.* **2016**, *263*, 1683–1701. [CrossRef] [PubMed]
16. Zhao, W.; Beers, D.R.; Appel, S.H. Immune-mediated Mechanisms in the Pathoprogression of Amyotrophic Lateral Sclerosis. *J. Neuroimmune Pharmacol.* **2013**, *8*, 888–899. [CrossRef] [PubMed]
17. Azam, S.; Haque, M.E.; Balakrishnan, R.; Kim, I.-S.; Choi, D.-K. The Ageing Brain: Molecular and Cellular Basis of Neurodegeneration. *Front. Cell Dev. Biol.* **2021**, *9*, 683459. [CrossRef]
18. Aigner, L.; Bogdahn, U. TGF-beta in neural stem cells and in tumors of the central nervous system. *Cell Tissue Res.* **2008**, *331*, 225–241. [CrossRef]
19. Cua, D.J.; Kastelein, R.A. TGF-β, a "double agent" in the immune pathology war. *Nat. Immunol.* **2006**, *7*, 557–560. [CrossRef]
20. Blank, U.; Karlsson, S. TGF-β signaling in the control of hematopoietic stem cells. *Blood* **2015**, *125*, 3542–3550. [CrossRef]
21. Kuespert, S.; Heydn, R.; Peters, S.; Wirkert, E.; Meyer, A.-L.; Siebörger, M.; Johannesen, S.; Aigner, L.; Bogdahn, U.; Bruun, T.-H. Antisense Oligonucleotide in LNA-Gapmer Design Targeting TGFBR2–A Key Single Gene Target for Safe and Effective Inhibition of TGFβ Signaling. *Int. J. Mol. Sci.* **2020**, *21*, 1952. [CrossRef] [PubMed]
22. Peters, S.; Kuespert, S.; Wirkert, E.; Heydn, R.; Jurek, B.; Johannesen, S.; Hsam, O.; Korte, S.; Ludwig, F.T.; Mecklenburg, L.; et al. Reconditioning the Neurogenic Niche of Adult Non-human Primates by Antisense Oligonucleotide-Mediated Attenuation of TGFβ Signaling. *Neurotherapeutics* **2021**, *18*, 1963–1979. [CrossRef] [PubMed]
23. Korte, S.; Runge, F.; Wozniak, M.M.; Ludwig, F.T.; Smieja, D.; Korytko, P.; Mecklenburg, L. Range of Neurological Signs in Cynomolgus Monkeys After Intrathecal Bolus Administration of Antisense Oligonucleotides. *Int. J. Toxicol.* **2020**, *39*, 505–509. [CrossRef] [PubMed]
24. Korte, S.; Luft, J.; von Keutz, A.; Runge, F.; Mecklenburg, L.; Wozniak, M.M.; Zander, S.; Ludwig, F.T.; Pajaziti, B.; Romeike, A.; et al. Save Your Maximum Tolerated Dose: How to Diagnose Procedure-Related Spinal Cord Lesions After Lumbar Intrathecal Bolus Administration of Oligonucleotides in Cynomolgus Monkeys. *Int. J. Toxicol.* **2020**, *39*, 510–517. [CrossRef]
25. Dhuri, K.; Bechtold, C.; Quijano, E.; Pham, H.; Gupta, A.; Vikram, A.; Bahal, R. Antisense Oligonucleotides: An Emerging Area in Drug Discovery and Development. *J. Clin. Med.* **2020**, *9*, 2004. [CrossRef]
26. Quemener, A.M.; Bachelot, L.; Forestier, A.; Donnou-Fournet, E.; Gilot, D.; Galibert, M.-D. The powerful world of antisense oligonucleotides: From bench to bedside. *Wiley Interdiscip. Rev. RNA* **2020**, *11*, e1594. [CrossRef]

27. Mazur, C.; Powers, B.; Zasadny, K.; Sullivan, J.M.; Dimant, H.; Kamme, F.; Hesterman, J.; Matson, J.; Oestergaard, M.; Seaman, M.; et al. Brain pharmacology of intrathecal antisense oligonucleotides revealed through multimodal imaging. *JCI Insight* **2019**, *4*, e129240. [CrossRef]
28. Peters, S.; Wirkert, E.; Kuespert, S.; Heydn, R.; Johannesen, S.; Friedrich, A.; Mailänder, S.; Korte, S.; Mecklenburg, L.; Aigner, L.; et al. Safe and Effective Cynomolgus Monkey GLP—Tox Study with Repetetive Intrathecal Application of a TGFBR2 Targeting LNA—Gapmer Antisense Oligonucleotide as Treatment Candidate for Neurodegenerative Disorders. *Pharmaceutics* **2022**, *14*, 200. [CrossRef]
29. Messina, S. New Directions for SMA Therapy. *J. Clin. Med.* **2018**, *7*, 251. [CrossRef]
30. Passini, M.A.; Bu, J.; Richards, A.M.; Kinnecom, C.; Sardi, S.P.; Stanek, L.M.; Hua, Y.; Rigo, F.; Matson, J.; Hung, G.; et al. Antisense oligonucleotides delivered to the mouse CNS ameliorate symptoms of severe spinal muscular atrophy. *Sci. Transl. Med.* **2011**, *3*, 72ra18. [CrossRef]
31. Engelhardt, J.A.; Fant, P.; Guionaud, S.; Henry, S.P.; Leach, M.W.; Louden, C.; Scicchitano, M.S.; Weaver, J.L.; Zabka, T.S.; Frazier, K.S. Scientific and Regulatory Policy Committee Points-to-consider Paper. *Toxicol. Pathol.* **2015**, *43*, 935–944. [CrossRef] [PubMed]
32. Frazier, K.S. Antisense oligonucleotide therapies: The promise and the challenges from a toxicologic pathologist's perspective. *Toxicol. Pathol.* **2015**, *43*, 78–89. [CrossRef] [PubMed]
33. Rippon, M.G.; Atkin, L.; Ousey, K.; Rippon, U. Autolysis: Mechanisms of action in the removal of devitalised tissue in wounds. *Br. J. Nurs.* **2016**, *25*, S40–S47.
34. Karaki, S. Paris, C., Rocchi, P. Antisense Oligonucleotides, A Novel Developing Targeting Therapy. *Antisense Ther.* **2019**, *10*, 1–19.